Vegetation Dynamics within the North American Monsoon Region

GIOVANNI FORZIERI

Dipartimento di Scienze della Terra, University of Florence, Florence, Italy

FABIO CASTELLI

Dipartimento di Ingegneria Civile e Ambientale, University of Florence, Florence, Italy

ENRIQUE R. VIVONI

School of Earth and Space Exploration, and School of Sustainable Engineering and the Built Environment, Arizona State University, Tempe, Arizona

(Manuscript received 14 May 2010, in final form 30 November 2010)

ABSTRACT

The North American monsoon (NAM) leads to a large increase in summer rainfall and a seasonal change in vegetation in the southwestern United States and northwestern Mexico. Understanding the interactions between NAM rainfall and vegetation dynamics is essential for improved climate and hydrologic prediction. In this work, the authors analyze long-term vegetation dynamics over the North American Monsoon Experiment (NAME) tier I domain (20°–35°N, 105°–115°W) using normalized difference vegetation index (NDVI) semimonthly composites at 8-km resolution from 1982 to 2006. The authors derive ecoregions with similar vegetation dynamics using principal component analysis and cluster identification. Based on ecoregion and pixel-scale analyses, this study quantifies the seasonal and interannual vegetation variations, their dependence on geographic position and terrain attributes, and the presence of long-term trends through a set of phenological vegetation metrics. Results reveal that seasonal biomass productivity, as captured by the time-integrated NDVI (TINDVI), is an excellent means to synthesize vegetation dynamics. High TINDVI occurs for ecosystems with a short period of intense greening tuned to the NAM or with a prolonged period of moderate greenness continuing after the NAM. These cases represent different plant strategies (deciduous versus evergreen) that can be adjusted along spatial gradients to cope with seasonal water availability. Long-term trends in TINDVI may also indicate changing conditions favoring ecosystems that intensively use NAM rainfall for rapid productivity, as opposed to delayed and moderate greening. A persistence of these trends could potentially result in the spatial reorganization of ecosystems in the NAM region.

1. Introduction

The North American monsoon (NAM) region in the southwestern United States and northwestern Mexico experiences seasonal greening of a range of ecosystems due to the synchronized availability of precipitation and solar radiation in the summer, July–September (JAS). Vegetation dynamics in parts of the NAM region have been explored using remote sensing observations and related to precipitation and soil moisture (Mora and Iverson 1998; Watts et al. 2007; Pennington and Collins 2007; Gómez-Mendoza et al. 2008; Vivoni et al. 2008a; Méndez-Barroso et al. 2009; Lizárraga-Celaya et al. 2010; Jenerette et al. 2010) and to climatic patterns, such as the El Niño–Southern Oscillation (ENSO), leading to rainfall anomalies (Salinas-Zavala et al. 2002; Weiss et al. 2004; Lotsch et al. 2005; Caso et al. 2007; Castro et al. 2009). Ecosystems themselves also strongly influence the land surface water and energy balance through their effects on radiation, rainfall interception, and the amount and partitioning of surface turbulent fluxes (e.g., Caparrini et al. 2003). As a result, the observed spatiotemporal dynamics in vegetation alter surface temperature and albedo (Méndez-Barroso and Vivoni 2010), and evapotranspiration (Vivoni

Corresponding author address: Enrique R. Vivoni, School of Earth and Space Exploration, Arizona State University, Bateman Physical Science Center, F-Wing, Room 650A, Tempe, AZ 85287-1404.
E-mail: vivoni@asu.edu

DOI: 10.1175/2010JCLI3847.1

et al. 2008a), with potential implications for the local recycling of precipitation in the NAM region (Anderson et al. 2004; Dominguez et al. 2008; Méndez-Barroso and Vivoni 2010).

Despite their important role, there is a lack of quantitative studies of vegetation dynamics in the major ecosystems in the entire NAM region. Salinas-Zavala et al. (2002) found interannual relations between the normalized difference vegetation index (NDVI), a measure of vegetation greenness, and precipitation anomalies associated with ENSO (winter) and the NAM (summer). The satellite dataset, from the Advanced Very High Resolution Radiometer (AVHRR), however, was not used to quantify the spatiotemporal vegetation patterns in the region or to identify potential landscape controls on the observed variability—for example, the role played by topography. The spatial distribution of vegetation dynamics is especially important in the NAM region as Coblentz and Riitters (2004) found a strong correspondence between vegetation and topographic features using a static land cover map derived from AVHRR. Their analysis, however, did not explore the temporal variations in the vegetation dynamics that are expected to occur along topographic gradients because of the strong interannual variability in NAM rainfall. Lizárraga-Celaya et al. (2010) used the enhanced vegetation index (EVI) from the Moderate Resolution Imaging Spectroradiometer (MODIS) to explore the latitudinal variation in seasonal vegetation phenology for different ecosystems in the NAM region and found higher peak EVI farther south in the domain. Their results, however, were limited to locations with in situ observations and did not address the spatial variability in vegetation phenological metrics within the region of complex terrain.

An important motivation for examining vegetation dynamics is the recent advances in quantifying precipitation in the NAM region using ground- and satellite-based platforms (e.g., Gochis et al. 2004, 2007; Hong et al. 2007; Gebremichael et al. 2007; Nesbitt et al. 2008). Improved monitoring has provided insights on precipitation intensity, duration, and frequency that have implications on vegetation dynamics. At regional scales, Gochis et al. (2007) and Brito-Castillo et al. (2010) illustrated north-to-south (latitudinal) variations in precipitation amounts and intensities that likely affect the spatial variations in the onset and duration of vegetation greening. Furthermore, several studies have identified strong topographic controls on precipitation characteristics. For example, Gochis et al. (2007), Gebremichael et al. (2007), and Nesbitt et al. (2008) found that high-elevation sites characterized by evergreen trees typically experience more frequent, but less intense, precipitation events as compared to lower-elevation sites in deciduous (subtropical and tropical) ecosystems. Thus, a closer inspection of the regional vegetation dynamics resulting from intraseasonal-to-interannual variability in NAM precipitation (and its associated spatial patterns) is warranted.

Remote sensing of vegetation dynamics may also serve to monitor spatial differences in seasonal precipitation in regions of limited ground data. Méndez-Barroso et al. (2009), for example, demonstrated that seasonal changes in MODIS-based EVI can depict spatial regions experiencing larger or smaller amounts of seasonal precipitation. Monsoons with higher regional rainfall typically result in a more intense vegetation response over a larger spatial extent. Furthermore, Méndez-Barroso et al. (2009) found a relatively strong correlation between precipitation amount and a measure of seasonal biomass productivity—namely, the time-integrated EVI (iEVI)—across a range of ecosystems. Developing diagnostic relations between seasonal precipitation and vegetation dynamics could provide knowledge on the spatial distribution of NAM rainfall, including its elevation dependence, for areas that are poorly monitored or inaccessible. Clearly, the phenological responses to seasonal rainfall characteristics are ecosystem dependent (e.g., Weiss et al. 2004; Watts et al. 2007; Vivoni et al. 2008a; Dominguez et al. 2008) such that inferences on precipitation need to be performed with care, in particular with respect to strong ecosystem variations with elevation.

Regional vegetation–topography relations have been explored in parts of North America using long-term remotely sensed databases (e.g., Riera et al. 1998; White et al. 2005; Deng et al. 2007). While topography alone does not dictate vegetation patterns, the strong correlations between atmospheric conditions and elevation in the NAM region lead to a clear spatial organization of ecosystems (Brown 1994). For example, Vivoni et al. (2007, 2008b) discussed the organization of precipitation, soil moisture, and vegetation along a mountain front in northwestern Mexico. Méndez-Barroso et al. (2009) later confirmed that vegetation dynamics varied considerably along this mountain front based on EVI data obtained from MODIS. Thus, a plausible hypothesis is that the observed vegetation patterns along semiarid mountain fronts are a result of variations in the soil water balance arising from elevation gradients in precipitation characteristics and in temperature regimes. One approach to test this hypothesis is through quantitative remote sensing of vegetation that can offer insight into topographic and geographic effects leading to ecosystem organization.

The spatiotemporal variations of vegetation would also be useful information to understand the potential influence of ecosystems on atmospheric processes during the NAM. While vegetation–climate linkages have been studied in North America (e.g., Pielke et al. 1998; Notaro

et al. 2006), a detailed analysis is lacking in the NAM domain. Dominguez et al. (2008) used NDVI data to corroborate that increases in evapotranspiration in the North American Regional Reanalysis (NARR; Mesinger et al. 2006) product leading to precipitation recycling were due to vegetation activity. Nevertheless, the NARR land surface model was forced with a 5-yr NDVI climatology (Gutman and Ignatov 1998) that does not capture interannual variations in vegetation activity. The interannual variations in the NAM ecosystems responses are particularly relevant in light of the work of Alessandri and Navarra (2008), which suggests that vegetation serves as a delayed biophysical memory to large-scale atmospheric teleconnections such as ENSO. While this linkage will not be explicitly discussed here, the spatiotemporal vegetation analysis provides a foundation for future climate studies in the NAM region interested in the vegetation–monsoon feedback.

In this study, we identify the spatiotemporal patterns of vegetation dynamics in the NAM region using a long-term remotely sensed NDVI dataset from AVHRR. Satellite-based vegetation indices are responsive to the availability of water and strongly correspond to ground-measured phenological events, in particular for semiarid regions (e.g., White et al. 1997; Maignan et al. 2008; Jenerette et al. 2010). Our aim is to provide a quantitative analysis of vegetation dynamics relevant to hydrologic and climate studies in the NAM region concerned with the role of ecosystems in modulating warm-season conditions at the land surface. In the study, we classify areas with similar vegetation dynamics (termed here as ecoregions) using the spatiotemporal variability of a set of vegetation metrics defined for the phenological growth season during the NAM. Ecoregions aid in identifying the large-scale topographic (elevation, slope, and aspect) and geographic (latitude and longitude) controls on the vegetation metrics. In addition, the ecoregion-averaged behavior is useful for assessing interannual variations in vegetation metrics. In particular, understanding the ecoregion-averaged behavior would help in developing techniques for scaling site observations over broader areas (Higgins and Gochis 2007; Méndez-Barroso and Vivoni 2010).

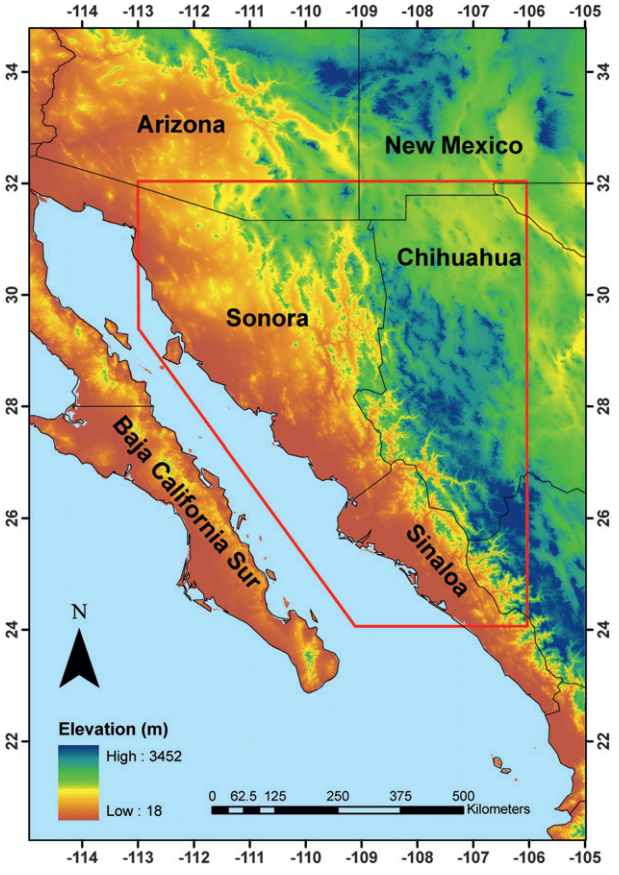

FIG. 1. The North American monsoon region in the southwestern United States and northwestern Mexico described by the 8-km DEM derived from USGS HYDRO1K. The entire extent is used for most analyses, while the red boundary is used to assess topographic and geographic controls.

2. Methods

a. Study region

The study region is a large domain that encompasses several states in the southwestern United States and northwestern Mexico (Fig. 1). The regional extent (20°–35°N, 105°–115°W) was selected to match the North American Monsoon Experiment (NAME) tier I domain (Higgins and Gochis 2007). The tier I domain was monitored for precipitation, surface fluxes, and atmospheric conditions during the NAME field campaign in 2004 and through subsequent efforts (see Vivoni et al. 2010a). The region is characterized by complex topography owing to the mountain ranges in the southern basin and range province, Madrean Archipelago, and the Sierra Madre Occidental (SMO; Coblentz and Riitters 2004). Terrain attributes are considered to exert controls on the spatial location of different ecosystems (e.g., Brown 1994; Vivoni et al. 2007, 2008b), in particular along mountain fronts with sharp changes in elevation. The mean annual precipitation varies considerably, ranging from approximately 100 to 800 mm and is determined by geographic position and elevation, with a varying proportion occurring during the NAM (e.g., Douglas et al. 1993; Vivoni et al. 2008a). While most analyses in this study encompass the entire NAME tier I domain, topographic and geographic controls are assessed for a smaller area (24°–32°N, 106°–113°W, see red polygon in Fig. 1) for clarity.

b. Remote sensing and land surface datasets

NDVI is a frequently used index to retrieve the phenological cycle and to quantify the spatiotemporal variability of vegetation (e.g., Reed et al. 1994; Zhang et al. 2003; Matsui et al. 2005; Watts et al. 2007; Forzieri et al. 2010). We used the Global Inventory Modeling and Mapping Studies (GIMMS) NDVI semimonthly dataset available from 1982 to 2006 at 8-km resolution, derived from the AVHRR sensor (Tucker et al. 2004). Two composites are available per month: 1) days 1–15 and 2) day 16 to the end of the month. AVHRR data at these resolutions has been widely used because of its long record length and its areal extent (e.g., Reed et al. 1994; Myneni et al. 1996; Kaufmann et al. 2000; Buermann et al. 2002; Zeng et al. 2003). The dataset has been corrected for sensor calibration, view geometry, volcanic aerosols, and other effects not related to vegetation (Pinzon et al. 2005; Tucker et al. 2005) and has shown to be stable with respect to interannual variations (Alcaraz-Segura et al. 2010). Preprocessing steps for the GIMMS NDVI included the following: 1) the masking of coastal and inland water bodies to focus the analysis over vegetated land areas; 2) the correction of missing values (0.37% of total) by linear interpolation of NDVI values in time; 3) the replacement of snow values, if any, with the most recent snow-free NDVI value; and 4) the identification and correction of outliers. Outliers were identified as NDVI values greater than three standard deviations from the long-term mean at a particular pixel and were corrected by linear interpolation in time.

In addition to the remotely sensed NDVI dataset, we gathered digital information on the study region through several sources. We characterized the regional topography at a spatial resolution coherent with the NDVI dataset using an 8-km spatially aggregated digital elevation model (DEM) from the United States Geological Survey (USGS) HYDRO1K dataset (original resolution of 1 km) (Verdin and Verdin 1999). Topographic attributes—such as elevation, slope, and aspect—were derived from the 1-km DEM and then aggregated to the 8-km resolution using a cubic interpolation. This procedure minimizes the potential errors associated with deriving terrain attributes from the coarse, 8-km DEM (e.g., Armstrong and Martz 2003; Vivoni et al. 2004). A static land cover map derived from Commission for Environmental Cooperation (1997) was used to characterize the regional ecosystems from the level II ecological classifications (see Dominguez et al. (2008) for a general description). Additional datasets including the coastlines, inland water bodies, and political boundaries were derived from the NAME database (available online at http://www.eol.ucar.edu/projects/name/).

Clearly, climate variables and their spatiotemporal distributions have a strong control on the regional vegetation dynamics (e.g., Coblentz and Riitters 2004; Méndez-Barroso et al. 2009; Jenerette et al. 2010). However, quantifying the relationships between vegetation and different climate conditions, such as temperature and precipitation, requires solving a number of data-processing and analysis issues related to the different spatiotemporal resolutions and the quality of available datasets in the United States and Mexico (see Zhu and Lettenmaier 2007). As a result, we selected in this study to focus on the relations between several metrics of vegetation dynamics and the terrain and geographic conditions in the region for which datasets exist with comparable spatial detail. Nonetheless, a description of the precipitation pattern in the region will aid in interpreting such relationships. To do this, we used the Climate Prediction Center (CPC) National Oceanic and Atmospheric Administration (NOAA) daily 1° gridded precipitation dataset (available online at http://www.cpc.noaa.gov). We assessed the reliability of this data with independent estimates from the Global Surface Summary of Day Database (GLOBALSOD, available online http://gcmd.nasa.gov). A consistency analysis was carried out using a total of 37 rain gauges. Results indicate the gridded precipitation product captured well the ground measurements (correlation values of ~0.75) and thus represents a suitable tool to investigate the spatiotemporal precipitation variations.

c. Methodology

1) Ecosystem detection through PCA and cluster analysis

To detect vegetation patterns, a classification procedure is performed in NDVI-derived feature space based on the principal component analysis (PCA). As NDVI exhibits temporal correlations, it is possible to transform the original time series into a set of standardized linear combinations through PCA. The PCA is a redundancy reduction technique that generates a new set of variables with which to describe the original dataset (Li and Kafatos 2000; Lillesand et al. 2008). As the vegetation dynamics are strongly affected by ecosystem-dependent seasonal components, we considered it useful to maintain the climatological means for each period in the PCA (Hirosawa et al. 1996). The scree graph method (Wilks 1995) is then used to detect the number of principal components that best describe the underlying spatiotemporal NDVI patterns. The set of the selected principal components represents the NDVI-derived feature space. The PCA images are subsequently normalized in the 0–1 range and processed through *K*-means cluster analysis (MacQueen 1967) using the squared Euclidean distance as an interclass distance measure, resulting in a set of clusters representing regional ecosystems. The *K*-means method has

been chosen in this study as a simple solution, characterized by short computation times, for the characterization of ecoregions. To examine the sensitivity of the procedure, the clustering process was tested with different numbers of classes. The number of clusters was determined by visually comparing the resulting classification map to the Commission for Environmental Cooperation (1997) ecosystem distributions.

2) PHENOLOGICAL CHARACTERIZATION USING VEGETATION METRICS

Several methods for the estimation of vegetation phenology from remote sensing data have been developed (Reed et al. 1994; White et al. 1997; Zhang et al. 2003). Explorative analysis was performed to detect the suitable method, including modality estimation using the slope method (Zhang et al. 2003). Modality refers to the number and timing of phenological peaks during a year and is important in areas with more than one precipitation season. To characterize modality, it is necessary to identify periods of NDVI increase and decrease associated with the annual phenological cycle. To do this, a moving window of five AVHRR compositing intervals was applied to the NDVI multiyear average. The multiyear average for each compositing period ($\mathrm{NDVI_{my}}$) is estimated as

$$\mathrm{NDVI_{my}}(m) = \frac{1}{N_y}\sum_{i=1}^{N_y}\mathrm{NDVI}[(i-1)\cdot M + m], \quad m = 1, \ldots, M \tag{1}$$

where i and m are indices of the year and the compositing period, N_y is the number of years (equal to 25), M is the number of the compositing periods per year (equal to 24), and NDVI(j) ($j = 1, \ldots, N_y \cdot M$) is the sequence of the original NDVI time series spanning from January 1982 to December 2006. Transitions from increasing to decreasing $\mathrm{NDVI_{my}}$ were identified for each pixel by a change from a positive to negative slope within a given window (and vice-versa). This reveals sharp increases (greening onset), decreases (greening offset), and $\mathrm{NDVI_{my}}$ peaks (maximum biomass production). As discussed in Zhang et al. (2003), growth cycles can be detected in this manner, including spring and summer greenup periods. The number of $\mathrm{NDVI_{my}}$ peaks indicates monomodal (only one peak) or multimodal (two or more peaks) vegetation dynamics. We estimated a set of vegetation metrics using a threshold method on the multiyear average NDVI. In pixels with more than one growing season (i.e., multimodality), we only capture the phenological cycle related to the NAM that tends to be the major growth period. In areas with multimodal dynamics, the selection of the NAM-related phenology is based on the following: 1) identifying the $\mathrm{NDVI_{my}}$ local minima between subsequent growing seasons and 2) extracting the NDVI images between the two local minima spanning the summer season.

To detect greening onset and offset, we transformed $\mathrm{NDVI_{my}}$ into a normalized ratio through the following pixel-based relationship (White et al. 1997):

$$\mathrm{NDVI_{ratio}}(m) = \frac{\mathrm{NDVI_{my}}(m) - \min(\mathrm{NDVI_{my}})}{\max(\mathrm{NDVI_{my}}) - \min(\mathrm{NDVI_{my}})}, \tag{2}$$

where $\mathrm{NDVI_{ratio}}(m)$ ranges from 0 to 1, and min and max represent the minimum and maximum values of $\mathrm{NDVI_{my}}(m)$ for the particular pixel of interest. Use of $\mathrm{NDVI_{ratio}}(m)$ allows for the accounting of variations in background reflectance among different sites and provides a normalization that is independent of vegetation type. Subsequently, a threshold T_n to identify the periods of greenness and the corresponding transitions (onset/offset) was selected based on a detailed sensitivity analysis. We analyzed means and standard deviation of greenness duration by varying the threshold values from 0.1 to 0.6 for each ecosystem (not shown). By comparing the results with the greenness duration tabulated in the literature (e.g., Eagleson 2002), we concluded that the threshold $T_n = 0.3$, lower than the value reported by White et al. (1997) of $T_n = 0.5$, better accounted for the rapid greenup in the NAM ecosystems.

As part of this analysis, seven vegetation phenological metrics were defined to characterize the ecosystem response to NAM precipitation: greening onset (TG) in day of year (DOY) or days; end or offset (TS) of the greenness period in days; total seasonal duration of the greenness period (DUR, days); maximum NDVI ($\mathrm{NDVI_{max}}$, dimensionless); time of the maximum NDVI ($\mathrm{TNDVI_{max}}$, days); within-monsoon range of the NDVI (ΔNDVI, dimensionless); and the time-integrated NDVI (TINDVI, days). Figure 2 depicts the vegetation metrics for two sampled pixels representing tropical dry forests (ECO-1) and mountain forests (ECO-2) selected because of their strong seasonal signal. The TG and TS of the greenness period were defined as the times when the $\mathrm{NDVI_{ratio}}$ time series matched the threshold $T_n = 0.3$. TG and TS represent antecedent and subsequent times to the peak, respectively, and are measured on a circular temporal scale. This can result in antecedent values of TS with respect to TG estimates, especially for vegetation dynamics with late summer or winter peaks. The DUR was derived by subtracting the onset and end times of the greenness period. The TINDVI was determined as the NDVI area between the onset and end of the greenness phase (Fig. 2). In this study, this was defined as

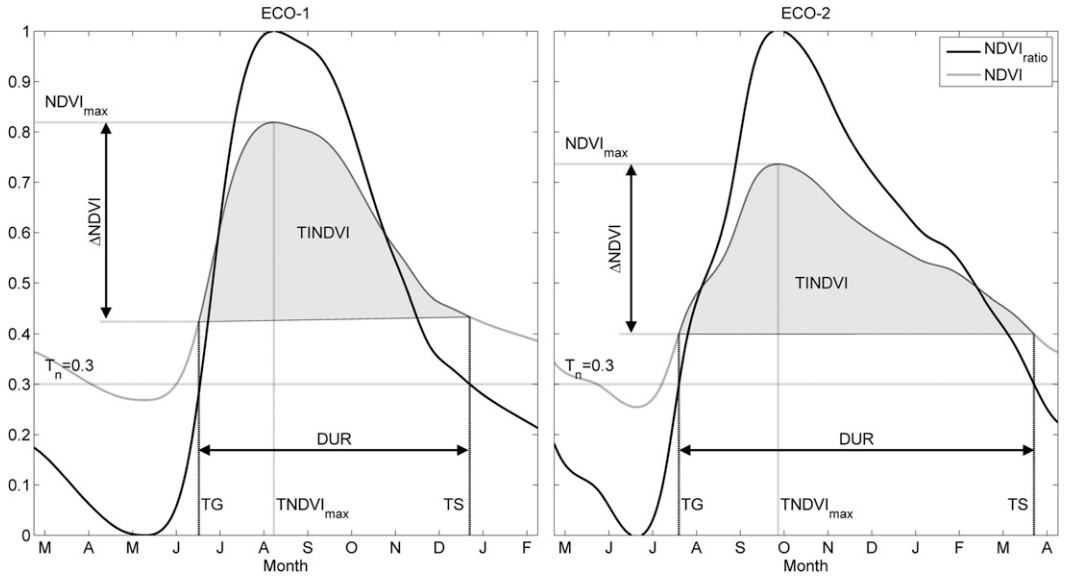

FIG. 2. Derivation of vegetation phenological metrics from the multiyear average NDVI (gray line) and the $NDVI_{ratio}$ (black line) at two sampled pixels belonging to two different ecoregions: (left) ECO-1 and (right) ECO-2. ECO-1 (26.13°N, 108.60°W pixel coordinates) is composed of tropical dry forests, while ECO-2 (23.58°N, 110.13°W pixel coordinates) is dominated by mountain woodlands and conifers.

$$\text{TINDVI} = \int_{\text{TG}}^{\text{TS}} \text{NDVI}\, dt + [\text{NDVI(TG)} - \text{NDVI(TS)}]\text{DUR}/2, \quad (3)$$

where dt is the integration time step, taken here as 1 day to avoid aliasing with the length of the compositing period. Since TINDVI accounts for the greening amount and its duration, this metric can be considered as a surrogate for the net primary productivity or biomass production in an ecosystem (Reed et al. 1994). While these remotely sensed metrics may not necessarily correspond to ground-based phenological events, they are used in this study as indicators of ecosystem dynamics in the region, as in Méndez-Barroso et al. (2009). Note that for synthesis purposes we have omitted results for TS. TS can be easily derived by adding DUR to TG.

3) INTERANNUAL VARIABILITY AND LONG-TERM TRENDS OF VEGETATION METRICS

To explore the interannual variability, we estimated the vegetation metrics for each year (1982–2006) by generating individual annual fields for each property. To reduce potential noise in the NDVI time series, we first applied a five-period moving average. This averaging allows a reduction of several NDVI data quality issues occurring at short time scales. The long-term interannual variability was estimated for each vegetation metric field at the pixel scale. In addition, a spatial average for each ecoregion was performed for each field. The number of pixels in each ecoregion is presented in Table 1. This resulted in a time series of the ecoregion-averaged temporal evolution of the vegetation metrics over the 25-yr study period from which interannual variations were assessed. To quantify ecoregion-averaged long-term trends, each time series was analyzed independently through a Mann–Kendall trend test with a 0.05 significance level. Additional linear trend tests for all the vegetation metrics were performed at the pixel scale based on the long-term dataset.

3. Results and discussion

a. Spatial and temporal variations in NDVI in the NAM region

The spatiotemporal variations in NDVI are first described in Fig. 3. The mean annual NDVI is computed as the long-term average of the annual mean NDVI, while the standard deviation of the mean annual NDVI represents the interannual variability. Interestingly, we found a variable correlation between mean annual NDVI and elevation quantified in terms of 0.58 and 0.29 Spearman's rank correlation for areas above and below 1200 MSL, respectively. Note the strong correspondence between the mean annual NDVI (Fig. 3a) and elevation (Fig. 1), with high NDVI (~0.6–0.7) for higher altitudes in Arizona, New Mexico, and the SMO in western Mexico. Northern mountains exhibit higher values in NDVI related to a sharp transition to conifers, while the SMO has a broader

TABLE 1. Statistical parameters of the vegetation metrics for each ecoregion, including the sample size (N). We used the following classification: tropical dry forests of the western Pacific coastal plain, hills, and canyons (ECO-1); mountain woodlands in the SMO composed of evergreen and deciduous forests (ECO-2); conifer forests in Arizona and New Mexico (ECO-3); semiarid grasslands, shrublands, and subtropical scrublands in the SMO piedmont (ECO-4); the Sonoran Desert (ECO-5); and the Chihuahuan Desert (ECO-6).

Vegetation metric	Statistical property	ECO-1	ECO-2	ECO-3	ECO-4	ECO-5	ECO-6
N		1420	1964	1666	2402	4948	4831
TG (DOY)	Mean	179.81	215.94	211.20	191.16	219.35	182.74
	Std	10.23	43.02	32.28	12.18	49.24	40.12
	Skewness	13.89	0.53	1.54	6.44	−0.63	−1.72
	Kurtosis	241.48	11.53	16.76	95.73	10.52	6.02
	Min	169	1	3	95	4	19
	Max	359	364	356	364	364	360
DUR (days)	Mean	197.93	260.30	192.58	153.57	253.58	145.56
	Std	47.20	45.42	67.80	38.57	58.62	43.23
	Skewness	0.19	−1.30	0.40	1.43	−1.28	1.67
	Kurtosis	1.61	4.35	2.08	4.34	3.09	4.90
	Min	94	116	21	97	105	93
	Max	287	331	332	294	338	310
ΔNDVI (dimensionless)	Mean	0.32	0.14	0.11	0.20	0.06	0.09
	Std	0.04	0.04	0.04	0.05	0.03	0.03
	Skewness	−0.84	1.24	0.60	0.66	1.40	0.19
	Kurtosis	3.30	5.03	3.38	2.62	4.56	2.37
	Min	0.19	0.03	0.03	0.11	0.03	0.03
	Max	0.40	0.34	0.21	0.39	0.17	0.20
$TNDVI_{max}$ (DOY)	Mean	244.26	256.19	248.31	241.72	175.39	243.90
	Std	15.01	74.23	43.17	10.36	102.34	15.67
	Skewness	0.44	−2.06	−2.83	0.73	−0.14	−5.35
	Kurtosis	2.25	6.42	14.86	2.98	1.25	55.07
	Min	217	7	22	217	7	82
	Max	277	352	352	277	352	277
$NDVI_{max}$ (dimensionless)	Mean	0.76	0.60	0.53	0.52	0.24	0.30
	Std	0.05	0.08	0.08	0.09	0.07	0.07
	Skewness	−1.04	−0.04	0.29	0.38	0.74	0.06
	Kurtosis	3.87	2.78	2.63	2.40	3.27	2.20
	Min	0.57	0.35	0.35	0.32	0.11	0.15
	Max	0.84	0.80	0.76	0.77	0.48	0.48
TINDVI (days)	Mean	120.95	140.46	91.56	65.40	54.49	38.12
	Std	30.52	35.62	33.41	17.92	18.18	14.02
	Skewness	0.27	−0.71	0.22	1.02	−0.13	1.24
	Kurtosis	1.96	3.02	2.01	3.78	2.83	4.78
	Min	37.40	51.38	9.82	33.80	15.87	15.94
	Max	187.96	206.28	169.96	138.52	114.21	107.83

increase in NDVI related to a more gradual change toward greener ecosystems. The lowest NDVI (~0–0.1) is found in the low desert regions of Arizona and Baja California and high deserts in New Mexico and Chihuahua that have high percentages of bare soil. While the correspondence of mean annual NDVI with elevation appears strong, it is noteworthy that coastal areas in Sinaloa and Sonora exhibit high NDVI, despite the relatively low elevations. This suggests that the elevation impact is modulated by a north–south (latitudinal) gradient in the mean annual precipitation (Fig. 3d). Similar spatial distributions of vegetation greenness were obtained through the geomorphologic analysis of Coblentz and Riitters (2004).

The interannual variability (Fig. 3b) is low, exhibiting values ranging from 0 to approximately 0.05, an order of magnitude smaller than the mean annual NDVI. Nevertheless, interesting spatial patterns can be observed, with the highest standard deviations found in 1) the foothills of the SMO characterized by an abrupt rise in elevations, 2) the Pacific coastal zones in Baja California, and 3) large agricultural sectors in Arizona, Sonora, and Sinaloa. The first set of sites are associated with the interannual variability of annual precipitation (Fig. 3e), as these areas are occupied by subtropical and tropical ecosystems that respond vigorously to summer rainfall (Fig. 3f). The overlap between precipitation and vegetation interannual variations is not exact, suggesting that precipitation alone cannot explain the interannual vegetation changes and ecosystem-specific responses occur. For example, Méndez-Barroso et al. (2009) found different greening strategies

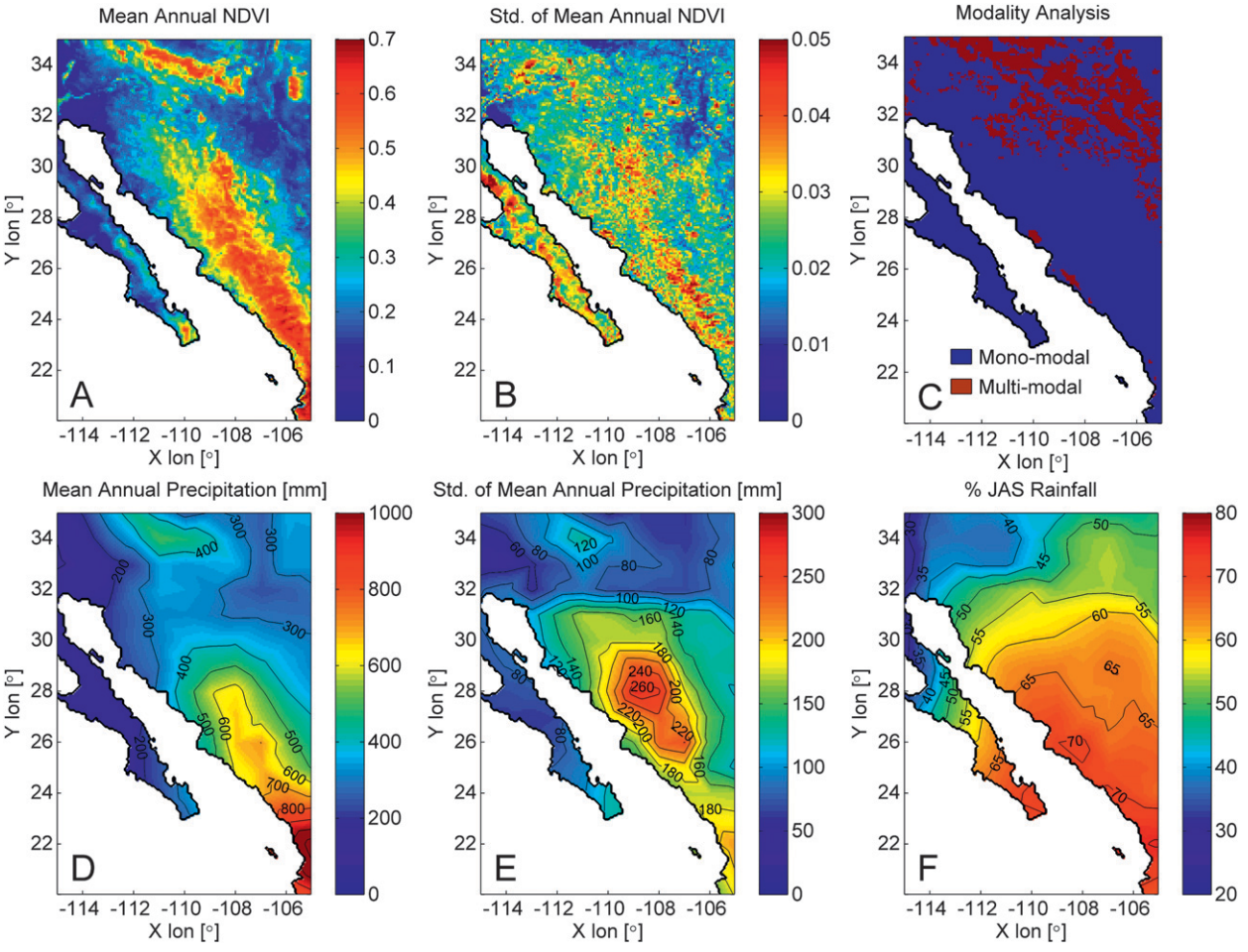

FIG. 3. (a) Mean annual NDVI, (b) standard deviation of mean annual NDVI, (c) vegetation modality, (d) mean annual precipitation, (e) standard deviation of mean annual precipitation, and (f) percentage of total annual rainfall occurring during the NAM (%JAS Rainfall) are shown.

between subtropical scrublands and evergreen woodlands to cope with interannual changes in summer rainfall. The second and third set of locations are likely not related to the NAM since the Pacific coastal sites have winter-dominated rainfall regimes (Douglas et al. 1993) and the agricultural areas are strongly dependent on irrigation water (e.g., Méndez-Barroso et al. 2008; Buyantuyev and Wu 2009).

The modality of the intraannual variation of vegetation (Fig. 3c) indicates that most of the region exhibits a single mode (monomodal) growth cycle related to the NAM. Multimodality within the NAM is only observed in 1) grassland and woodland areas in New Mexico and Arizona where both winter and summer rainfall lead to greening and 2) large agricultural areas where two or more annual crop rotations are possible in Sonora and Arizona. Grassland sites are typically characterized by a spring growth season (April–May) following winter precipitation and a more intense, late summer growth (August–October) after the NAM onset, as shown, for example, in Pennington and Collins (2007) and Ivanov et al. (2008). The predominance of monomodal vegetation dynamics in the NAM region, in particular within Mexico, justifies our focus on vegetation metrics derived from phenological changes during the summer in the following.

b. *Identification and characteristics of ecoregions in the NAM domain*

The principal component analysis of the AVHRR NDVI dataset revealed that the first three principal components (PCs) explain 90.91% of the sample variance, with a large proportion in the first PC (PC1: 83.23%, PC2: 5.87%, and PC3: 1.81%). Figure 4 shows the three principal components of NDVI, yielding a set of spatial patterns describing regions where vegetation dynamics tend to be highly correlated. To help interpret these patterns,

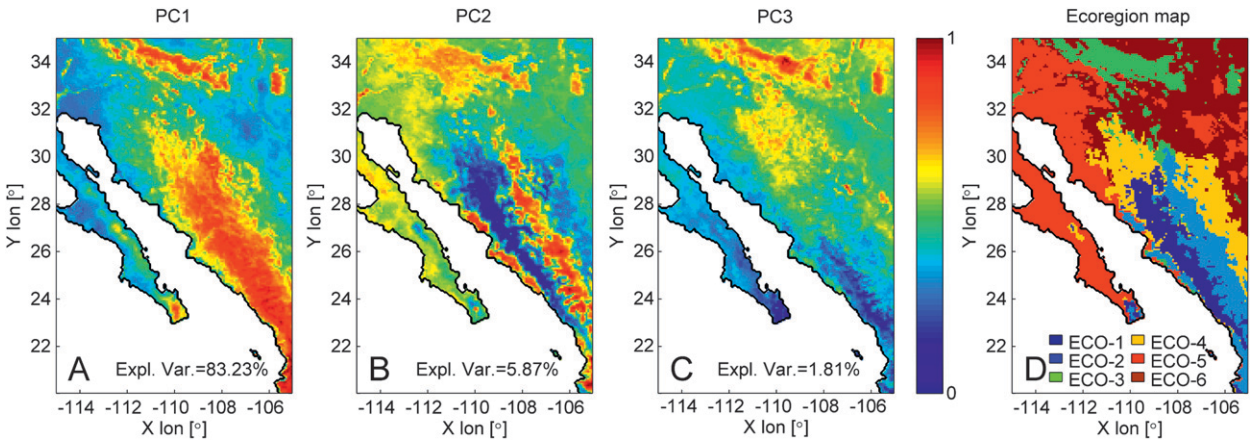

FIG. 4. Normalized PCs: (a) PC1, (b) PC2, and (c) PC3, with (d) the ecoregion map obtained through the *K*-means cluster analysis.

Fig. 5 presents the principal component loadings (L-PC) associated with each spatial mode. These loadings describe the temporal correlation between the principal component and each of the original NDVI images. Seasonal, interannual, or long-term trends in the L-PCs are indicative of the relative changes in the explanatory strength of the principal components.

PC1 is strongly related to mean annual NDVI (Fig. 3a), indicating the annually averaged greenness is the most important discriminant. PC1 reflects both topographic and geographic controls on climatic conditions that lead to different ecosystems in the NAM region. Temporal variations in PC1 loadings (Fig. 5) exhibit low seasonality, suggesting the PC1 is not related to NAM precipitation but rather to ecosystem characteristics (Fig. 3a). PC2, on the other hand, exhibits a spatial pattern related to the seasonal changes of NDVI. Note, for example, that a sharp contrast is observed between high-elevation evergreen areas (red colors) with a low NDVI range and intermediate-elevation sites (blue colors) occupied by

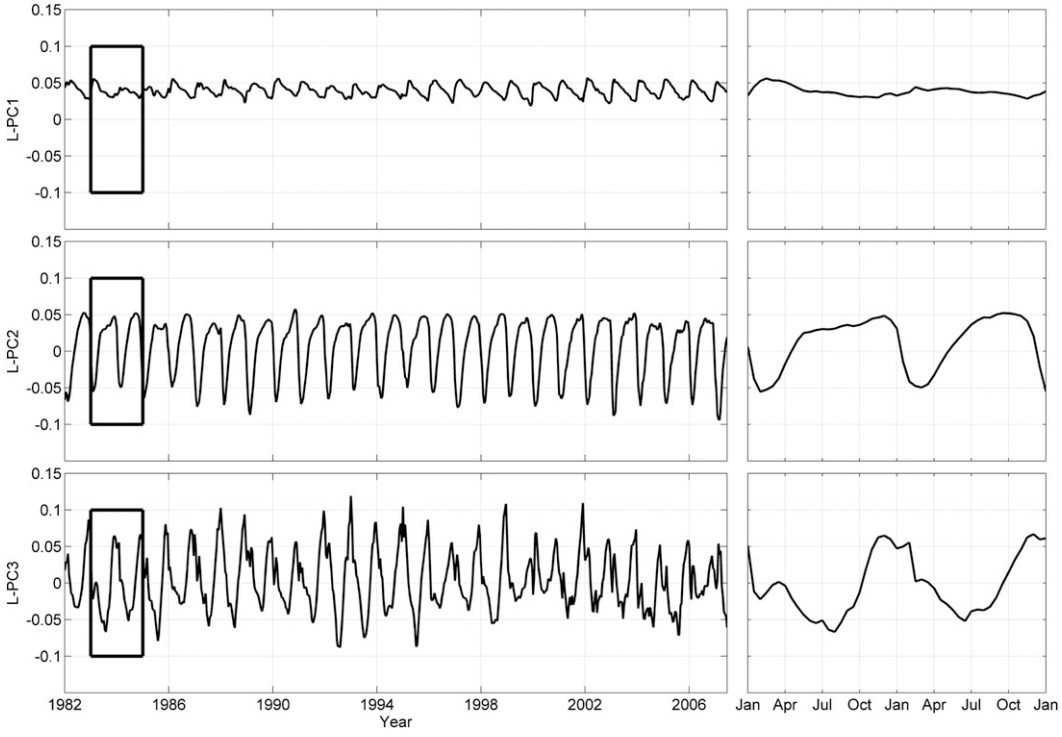

FIG. 5. (left) L-PC associated with the spatial modes. The *y* axis is the degree of correlation, while the *x* axis indicates time. (right) Detailed variations of L-PCs during a 2-yr period in a sequence.

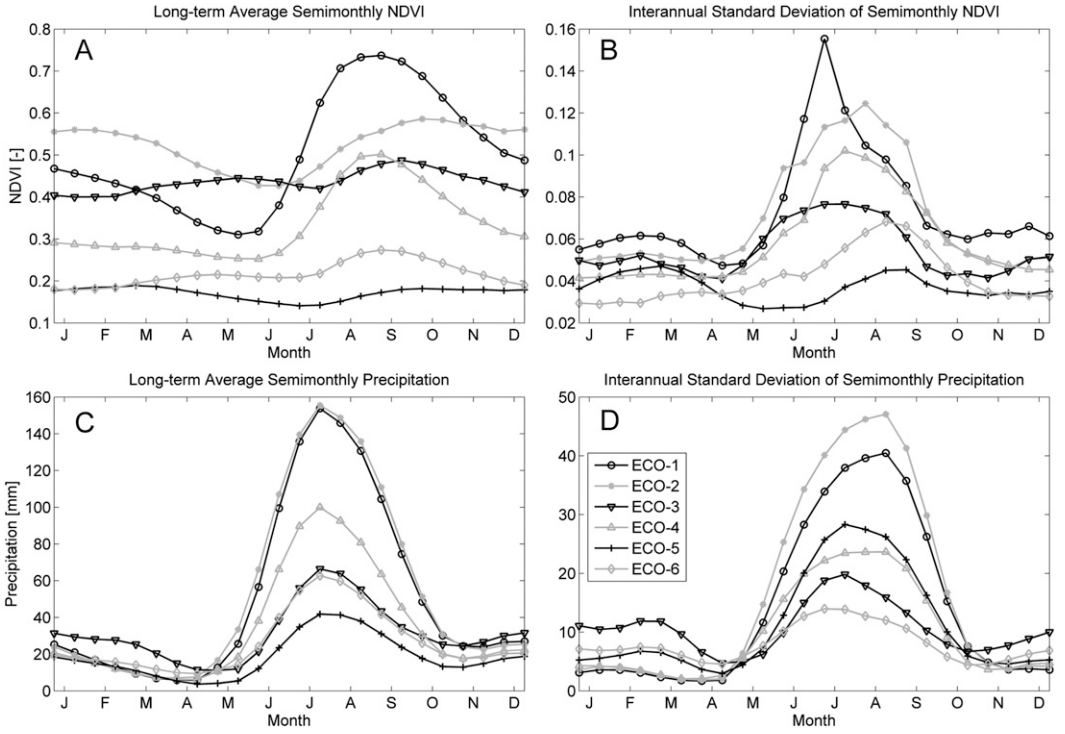

FIG. 6. (a) Long-term averaged NDVI, (b) interannual standard deviation of NDVI, (c) long-term averaged precipitation, and (d) interannual standard deviation of precipitation within each ecoregion (semimonthly composites).

highly seasonal ecosystems with a greater NDVI range. This is confirmed by PC2 loadings (Fig. 5) that exhibit a strong seasonal variation due to NAM precipitation. Finally, PC3 presents a spatial pattern driven by latitude and proximity to the coast. For example, a clear distinction is observed along 26°N on the mainland, while a more gradual latitudinal change is present in Baja California. Interestingly, PC3 loadings (Fig. 5) exhibit the largest interannual variations, which could be related to long-term changes in phenological cycles.

Based on the PCA, we utilized cluster analysis to perform the ecosystem classification shown in Fig. 5d. We compared the ecoregions with the land cover map of the Commission for Environmental Cooperation (1997) finding excellent agreement. In addition, the ecoregion map shares similarities with the ''study areas'' of Salinas-Zavala et al. (2002) and with the classifications of Brown (1994). ECO-1 represents the tropical dry forests of the western Pacific coastal plain, hills, and canyons and matches areas with high NDVI range in PC2 (Fig. 4b, blue colors). ECO-2 captures mountain woodlands in the SMO composed of evergreen and deciduous forests and coincides with low NDVI range in PC2 (Fig. 4b, red colors). While ECO-1 and ECO-2 primarily occur in the SMO, some areas in Baja California exhibit similar dynamics. ECO-3 is closely associated with conifer forests in Arizona and New Mexico that have high mean annual NDVI (PC1). ECO-4 is composed of semiarid grasslands, shrublands, and subtropical scrublands in the SMO piedmont with monomodal dynamics. This semiarid region transitions toward the North American deserts in ECO-5 and ECO-6. Note that ECO-5 is more representative of the Sonoran Desert, while ECO-6 captures the Chihuahuan Desert, though the distinction between these deserts is uncertain based on the vegetation dynamics, as in Salinas-Zavala et al. (2002). It is important to note that the ecoregion classification yields a limited number of areas in which the intraclass variability is low compared to the interclass differences. We would expect, however, that mixtures of vegetation types are possible within an ecoregion. For example, ECO-4 contains a mixture of grasslands, shrublands, and subtropical scrublands that span two different areas to the north and east of the Sierra Madre Occidental.

Figure 6 presents the seasonal variation of the long-term means and interannual standard deviations of NDVI and precipitation for each ecoregion. Three ecoregions exhibit strong seasonal fluctuations (ECO-1, ECO-2, ECO-4), with low NDVI in the spring and a vegetation peak in the summer or fall associated with the NAM (Figs. 6a,c). Seasonality of the tropical dry forests and semiarid ecosystems (ECO-1, ECO-4) is tuned to the NAM onset and offset, while mountain woodlands (ECO-2) exhibit

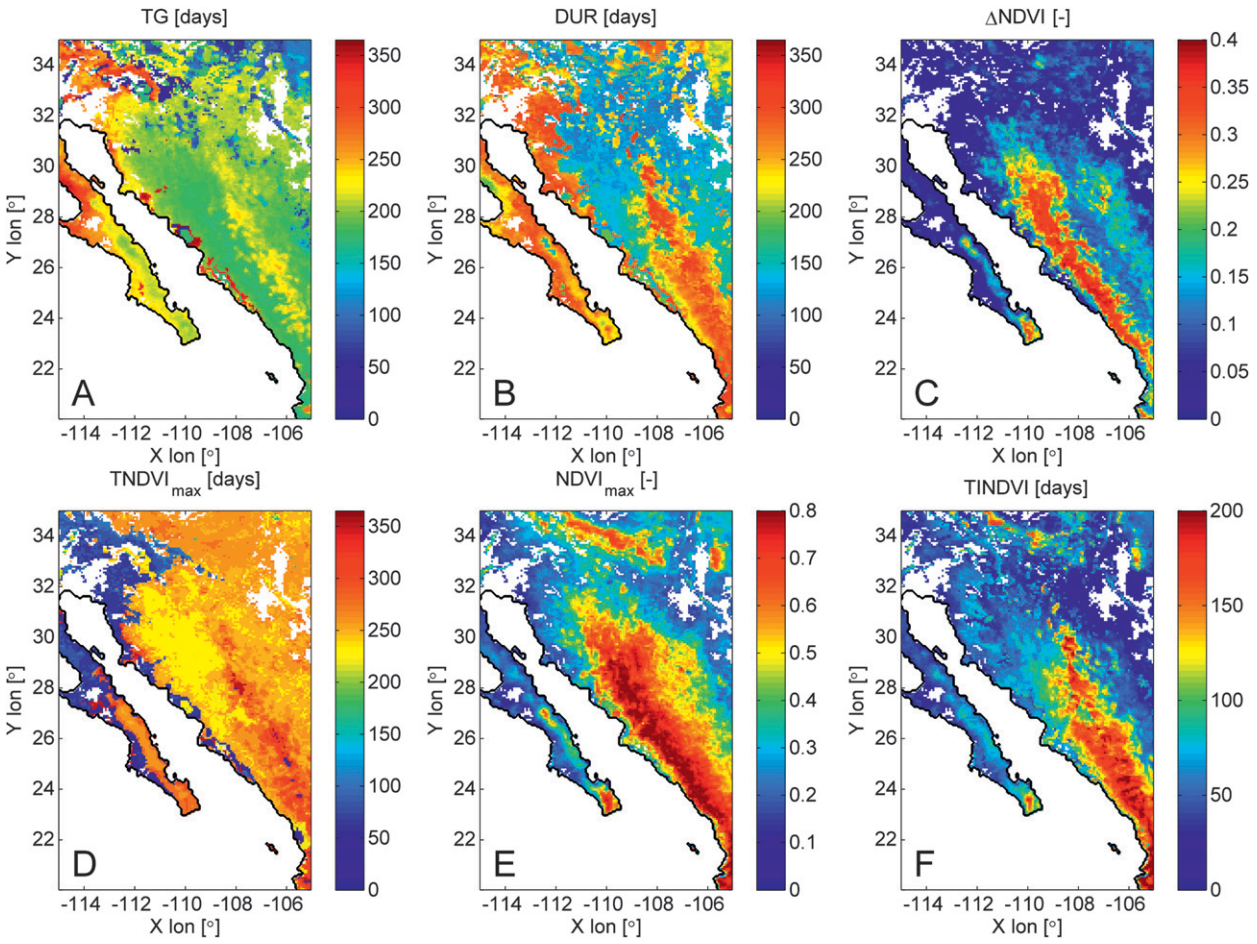

FIG. 7. Spatial distributions of the time-averaged vegetation metrics: (a) TG, (b) DUR, (c) ΔNDVI, (d) $TNDVI_{max}$, (e) $NDVI_{max}$, and (f) TINDVI. Areas with no NDVI seasonality are masked (white regions). Note that DOY = 1 (1 Jan) and DOY = 365 (31 Dec) for TG and $TNDVI_{max}$ are adjacent in time but may show strong variations in the coloration because of the selected scheme.

a delayed response to summer rainfall (see Méndez-Barroso et al. (2009) for a discussion). The other ecoregions (ECO-3, ECO-5, ECO-6) have more limited seasonality, owing to their composition of conifer forests (ECO-3) or desert vegetation (ECO-5, ECO-6), though ECO-6 responds to the NAM. The relative seasonality of the Sonoran (ECO-5) and Chihuahuan (ECO-6) Deserts is difficult to assess because of the mixture of ecosystem distributions. While these areas do not exhibit strong seasonality on average, Figs. 6b,d reveal that NAM rainfall does induce strong year-to-year differences even for the desert and conifer regions. Overall, the interannual variability is largest from June to October across all ecoregions, suggesting a relation to annual differences in timing, duration, and magnitude of the NAM (e.g., Higgins and Shi 2001; Gutzler 2004). Ecoregions with the largest interannual variability (ECO-1, ECO-2, ECO-4) coincide with drought–deciduous ecosystems that depend most strongly on the NAM. These ecoregions also coincide strongly with the ''core region'' of interannual NAM variability defined by Gutzler (2004). Clearly, ecoregions help to summarize a set of complex spatiotemporal vegetation dynamics resulting from seasonal and interannual variations in precipitation forcing.

c. *Spatial variations of vegetation phenological metrics*

Vegetation metrics during the NAM are a succinct means to understand the spatiotemporal variations in phenology (Reed et al. 1994). Figure 7 shows the time-averaged spatial patterns of TG (Fig. 7a), DUR (Fig. 7b), range of NDVI (ΔNDVI, Fig 7c), $TNDVI_{max}$ (Fig. 7d), $NDVI_{max}$ (Fig. 7e), and TINDVI (Fig. 7f). Spatial maps are complemented by statistical metrics for each ecoregion in Table 1, including the spatial mean, standard deviation (std), skewness, kurtosis, minimum (min), and maximum (max) values. These statistics represent conditions in each ecoregion and thus are robust estimates based on large

sample sizes (N, number of pixels in Table 1). The statistics also allow inspection of the relation between properties of the spatial distributions in each ecoregion. For example, a strong linear (positive) relation exists between the spatial std and mean TINDVI (slope = 0.22; $p < 0.01$), indicating that ecoregions with greater TINDVI also exhibit stronger spatial variations.

The onset of NAM vegetation greening typically begins on DOY 180–220 (July–August), with relatively low spatial variability among ECO-1, ECO-2, and ECO-4 (Fig. 7a, Table 1). A clear delay in TG is observed for conifer forests in ECO-2, relative to tropical dry forests in ECO-1. In addition, peripheral areas to the NAM region exhibit strong differences in TG, including sites with growing seasons in the spring (e.g., grasslands in ECO-6) or fall (e.g., coastal ECO-5 areas). TG is an excellent indicator of ecosystems (yellow and green in Fig. 7a) with a strong dependence on summer rainfall, and it thus delimits the NAM region in terms of vegetation phenology. In addition, TG shows a signature of the later onset of the NAM from north to south (Higgins and Shi 2001), with ECO-1 having an earlier vegetation onset compared to ECO-4. A complementary measure to the onset time is the duration of greening (Fig. 7b), which exhibits mean lengths of 150 (ECO-4)–260 days (ECO-2). Note that DUR can distinguish between high-elevation forests (red, high DUR) and intermediate-elevation grasslands and dry forests (blue, low DUR) along the SMO. In fact, higher seasonality (low DUR) is observed in ecosystems (ECO-1, ECO-4, ECO-6) that are more dependent on the NAM rainfall and exhibit drought–deciduous phenology. For these ecoregions, DUR is substantially longer farther south in the NAM region, indicating that the TS is more sensitive than TG to latitudinal variations in the NAM.

An important measure of seasonal greening is the range of NDVI (Fig. 7c) as this indicates ecosystems with more abrupt changes. A coherent spatial pattern of high ΔNDVI is centered at the SMO foothills (ECO-1) and extends into semiarid highlands (ECO-4), with smaller ΔNDVI for high-elevation evergreen forests (ECO-2). The mean values of ΔNDVI across the ecoregions range from 0.06 (ECO-5) to 0.32 (ECO-1), with relatively low spatial variations (std from 0.03 to 0.05) across all ecoregions (Table 1). This indicates that ΔNDVI can help identify subtropical and tropical ecosystems whose phenology is well tuned to NAM rainfall through leafing on of large plant canopies (e.g., Pérez-Ruiz et al. 2010; Vivoni et al. 2010c). When compared to $NDVI_{max}$ (Fig. 7e), it is clear that ΔNDVI is a large fraction of the maximum NDVI observed in response to the NAM. Note that $NDVI_{max}$ exhibits a spatial distribution that is closely tied (but not identical) to the mean annual NDVI and PC1 (Figs. 3a and 4a). Furthermore, ecoregion values of $NDVI_{max}$ range from 0.24 (ECO-5) to 0.76 (ECO-1), such that $\Delta NDVI/NDVI_{max}$ varies from 0.25 to 0.42. As with ΔNDVI, spatial variations of $NDVI_{max}$ in each ecoregion are low, with coefficient of variations (CV) from 0.07 (ECO-1) to 0.29 (ECO-5), and they are stronger for areas with lower maximum greening. This strong, coherent change in NDVI is a signature of the transformation from desert to lush green conditions in the region (e.g., Watts et al. 2007; Vivoni et al. 2008a).

The timing of the maximum NDVI varies spatially in the NAM region (Fig. 7d). Overall, the peak greenness is typically during late August–early September (ECO-1, ECO-2, ECO-3, ECO-4, and ECO-6), well after the NAM onset. In contrast, portions of ECO-5 have winter/spring growth peaks that impact the spatial average $TNDVI_{max}$ and lead to a large ecoregion variation (Table 1). As compared to TG, $TNDVI_{max}$ exhibits stronger variations with latitude along the SMO foothills and with elevation within the SMO. This shows that subtropical scrublands and tropical dry forests (ECO-4, ECO-1) have later peak greenness at latitudes less than 26°N and earlier $TNDVI_{max}$ for northern latitudes (26°–32°N). This delay in $NDVI_{max}$ for southern locations is likely due to the progression of the month of maximum rainfall from July to August to September over these latitudes (Brito-Castillo et al. 2010). Furthermore, the delay in $TNDVI_{max}$, for a similar TG, leads to a longer DUR of the seasonal greening for southern areas. A similar delay in $TNDVI_{max}$ and an increase in DUR occur for higher-elevation sites in ECO-2, with some locations with conifer woodlands having peak greenness in the fall or winter period.

The time-integrated NDVI (Fig. 7f) is a useful indicator of the total biomass fixed during the growth season and is related to the net primary productivity (Reed et al. 1994). The spatial distribution of TINDVI suggests that more productive ecosystems are located in the tropical dry forests of ECO-1 and the evergreen and deciduous woodlands of ECO-2 and ECO-3 (Table 1). Significantly smaller TINDVI, on the order of 50% less, occurs in semiarid grasslands, shrublands, and subtropical scrublands (ECO-4, ECO-5, ECO-6). Interestingly, TINDVI exhibits a latitudinal gradient with higher values in the southern areas and appears to combine the spatial features of the DUR and ΔNDVI distributions (Figs. 7a and 7c). This suggests that high values of TINDVI can be achieved in two different ways: 1) with a short period of intense greening (e.g., tropical dry forests, ECO-1) or 2) with a prolonged period of moderate greenness (e.g., evergreen or conifer forests, ECO-2, ECO-3). In the first case, the ecosystem response is well

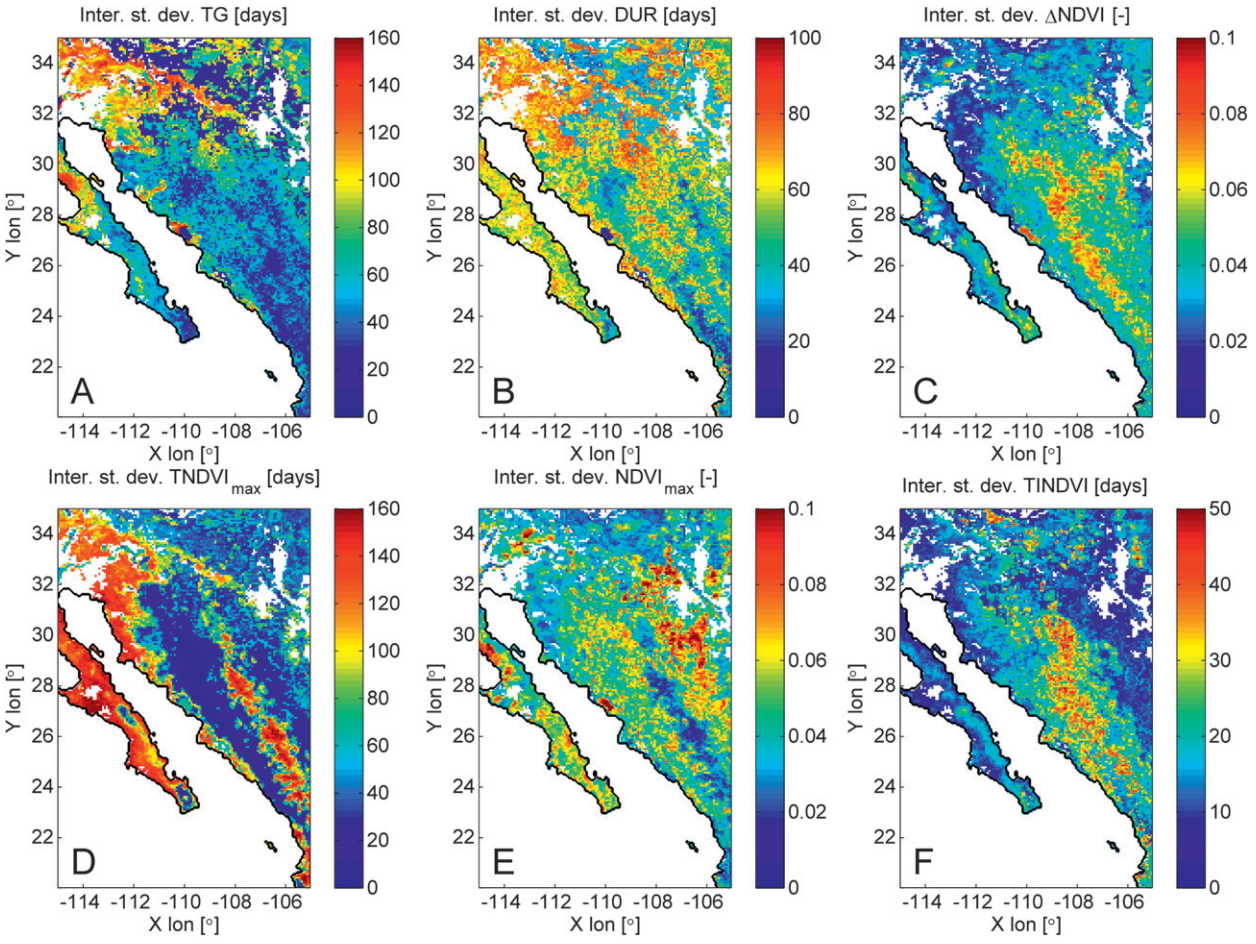

FIG. 8. Spatial distribution of the interannual standard deviation of the vegetation metrics: (a) TG, (b) DUR, (c) ΔNDVI, (d) $TNDVI_{max}$, (e) $NDVI_{max}$, and (f) TINDVI.

tuned to rainfall availability and the greening TS begins rapidly after the monsoon ends (Fig. 6a). In the second case, moderate greening occurs in response to the NAM, but it continues well after the end of the season in part because of the impact of soil moisture memory. These two cases represent different plant strategies to cope with the seasonal water availability. Thus, TINDVI is an appropriate metric to quantify seasonal biomass productivity, but its value should be inspected along with DUR and ΔNDVI, as different plant strategies can lead to similar results.

d. Interannual variations of spatial phenological metrics

To complement the time-averaged patterns, we present the interannual variations of the vegetation metrics in Fig. 8. TG exhibits low year-to-year differences farther south in the domain for all ecoregions indicating a more consistent response to NAM rainfall (Fig. 8a). Interestingly, some desert and conifer areas (ECO-6, ECO-3) also have low variations of TG, possibly due to consistent greening onset related to temperature increases. The highest interannual variability of TG occurs for areas in ECO-5 with a winter rainfall component that is more susceptible to ENSO. Interannual changes in greening duration (Fig. 8b) reflect the patterns of TG in ecoregions above 30°N, but they are quite different in southern sites. In particular, large year-to-year differences in ECO-2 and ECO-4 show variations in greening TS since TG changes are low. This suggests that high-elevation sites vary their senescence period depending on the precipitation available in fall and winter to sustain greenness. As a final timing metric, $TNDVI_{max}$ (Fig. 8d) provides a clear distinction between ecosystems with consistent peak greening times (ECO-1, ECO-3, ECO-4, ECO-6) and those with strong variations from year to year (ECO-2, ECO-5). Given the correspondence with Fig. 7d, it is evident that ecosystems with a strong dependence on NAM rainfall have consistent

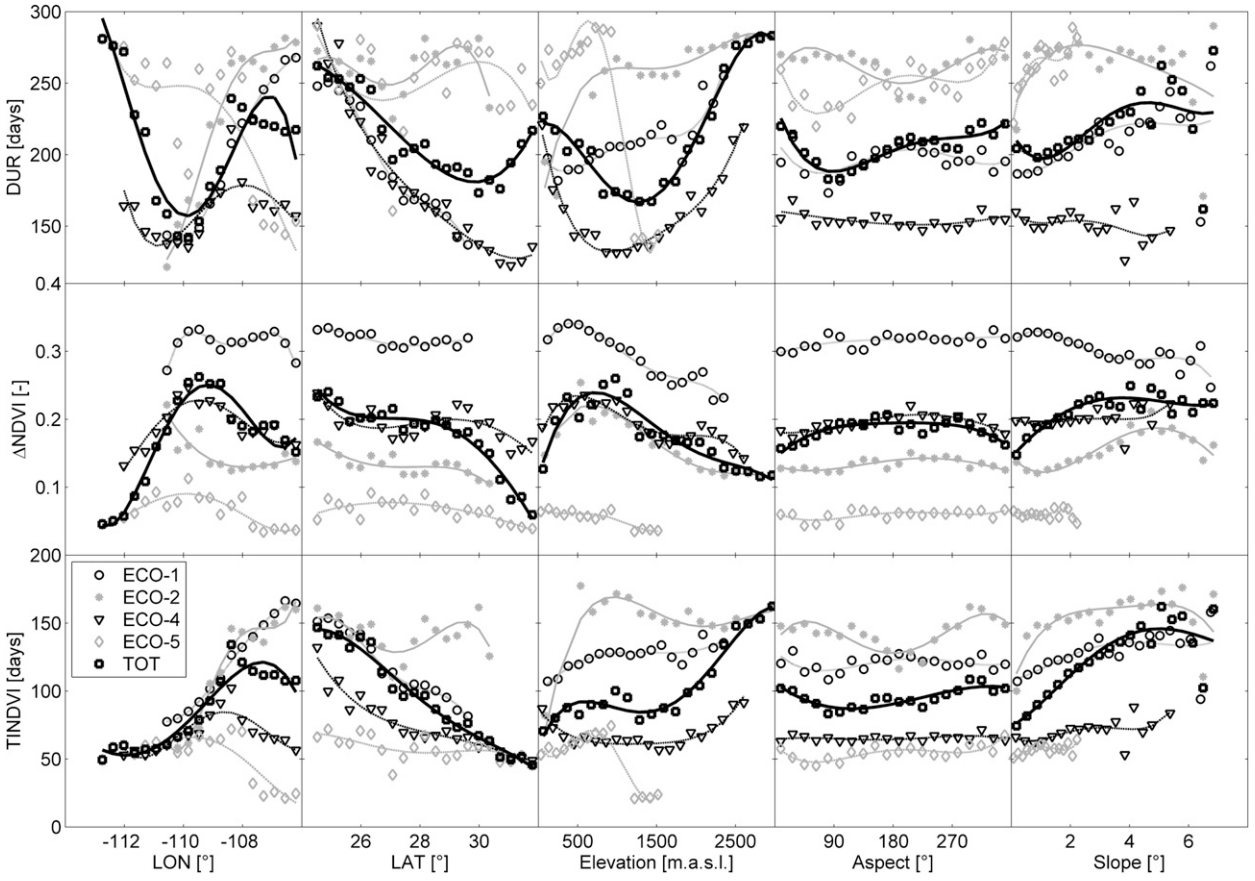

FIG. 9. Relations between DUR (days), ΔNDVI (dimensionless), and TINDVI (days) with latitude, longitude, elevation, aspect, and slope for four ecoregions (ECO-1, ECO-2, ECO-4, and ECO-5) and the entire red polygon in Fig. 1 (TOT). Averaged values were derived using bins that spanned the sampled range. Bin sizes are 0.4° for latitude, longitude, and slope; 18° for aspect; and 150 m for elevation. For improved visualization, the best-fit polynomial relations were added to depict the overall trends.

peak timings, while areas with either stronger winter rainfall (ECO-5) or sustained greening after the NAM (ECO-2) have much higher variations from year to year.

The interannual variations of the vegetation magnitude metrics (ΔNDVI and $NDVI_{max}$) exhibit less clear spatial patterns (Figs. 8c and 8e) as compared to the timing metrics. Note that tropical dry forests (ECO-1) exhibit the highest year-to-year differences in ΔNDVI (~0.07–0.1), yet moderate changes in $NDVI_{max}$ (~0.04–0.06), suggesting these ecosystems have variations in the minimum NDVI. Similarly, mountain conifers (ECO-2) have modest differences in ΔNDVI (~0.04–0.06) and very low changes in $NDVI_{max}$ (<0.02). As a result, these two plant strategies (deciduous versus evergreen) have similar directional responses (of different magnitude) to interannual differences in NAM rainfall, to reduce the minimum NDVI prior to or after the NAM, while maintaining the peak greenness amounts. The interannual fluctuations of TINDVI (Fig. 8f) closely follow the spatial pattern of the annually averaged values (Fig. 7f), indicating that the most productive ecosystems (higher biomass) also have the highest year-to-year variations. Based on the previous discussion, large TINDVI changes likely result from either (i) adaptations of ΔNDVI in deciduous ecoregions or (ii) modifications to DUR in evergreen ecosystems.

e. *Geographic and topographic controls on biomass productivity*

We explore the geographic and topographic variations of the time-averaged DUR, ΔNDVI, and TINDVI in Fig. 9. Understanding these controls on vegetation activity should reveal overall trends associated with ecosystem adaptations to precipitation availability. We selected a smaller domain, encompassing ECO-1, ECO-2, ECO-4, and ECO-5, to focus on the core of the NAM region (red polygon in Fig. 1). Results are shown for each ecoregion and for the entire selected area (labeled TOT). Variations in these metrics are explored as a function of latitude and longitude to reveal possible effects related to 1) photoperiod changes (day and season length) and 2) variations in

TABLE 2. Statistical parameters of the topographic features for each ecoregion. Slope and aspect are defined as the angles (°) of the surface normal upward from the horizontal direction and clockwise from north, respectively.

Topographic metric	Statistical property	ECO-1	ECO-2	ECO-3	ECO-4	ECO-5	ECO-6
Elevation (m)	Mean	716.32	1782.70	1443.00	1310.80	482.66	1290.80
	Std	473.94	866.49	610.03	663.12	454.28	330.05
	Skewness	0.87	−1.13	−1.19	−0.19	0.79	−0.86
	Kurtosis	3.37	2.90	3.85	1.85	2.23	4.40
	Min	51.14	5.50	5.66	0.00	0.00	0.00
	Max	2677.60	3041.90	2598.80	2674.60	1963.00	2427.90
Slope (°)	Mean	1.60	1.41	1.62	1.05	0.48	0.76
	Std	1.19	1.24	1.09	0.76	0.39	0.62
	Skewness	1.23	1.42	0.61	1.60	1.48	1.98
	Kurtosis	4.47	5.01	2.84	6.99	6.12	8.40
	Min	0.03	0.00	0.00	0.00	0.00	0.02
	Max	6.92	7.01	4.71	6.14	3.07	4.42
Aspect (°)	Mean	209.33	194.76	207.78	174.94	204.48	170.73
	Std	79.20	99.84	102.07	95.51	83.06	101.85
	Skewness	−0.67	−0.44	−0.63	−0.01	−0.72	0.07
	Kurtosis	2.84	2.04	2.05	1.83	2.97	1.63
	Min	0.32	0.00	0.46	0.08	0.00	0.00
	Max	359.83	359.70	350.34	359.89	359.16	359.01

the distance to the Gulf of California. Topographic attributes (elevation, aspect, and slope) were used to identify if terrain properties impact the spatial distribution of DUR, ΔNDVI, and TINDVI. While elevation is known to impact ecosystem distributions in the NAM region, less is known on the effects, if any, of terrain slope and aspect, as observed in other areas (White et al. 2005; Chen et al. 2007). For each variable, spatial averages in the metrics were derived using bins that spanned the sampled ranges. For reference, Table 2 presents the terrain attributes of each ecoregion.

The variation of the metrics with longitude is considerable for all ecoregions as the distance from the coast affects elevation and proximity to the moisture source. In general, TINDVI increases east from the coastal areas. For ECO-1 and ECO-2, TINDVI doubles in magnitude from coastal (−111°W) to mountain areas (−106°W). It is interesting to note that the increases in TINDVI are primarily due to higher DUR farther east since ΔNDVI is relatively constant with longitude in ECO-1 and ECO-2. The longitudinal variation in TINDVI, however, is partly affected by concurrent latitudinal changes since ECO-1 and ECO-2 are organized from northwest to southwest. As a result, the isolated longitudinal control is likely to be smaller, though still present (Fig. 7f). Note also that TINDVI in ECO-1 and ECO-2 converges to the low values in ECO-4 and ECO-5 along their western extents. Interestingly, ECO-4 and ECO-5 have a peak of TINDVI near 109°W, with decreasing levels eastward that are a result of changes in ΔNDVI. This behavior is likely due to the rain shadow effects of the SMO with greater vegetation activity on the western side (ECO-1) as compared to the continental interior (ECO-4) where vegetation productivity is reduced.

Latitudinal position also plays an important role in the metrics, with more productive ecosystems in terms of TINDVI in each ecoregion in the southern latitudes (24°–26°N). The strongest latitude effects are observed for ECO-1 (tropical dry forest) and ECO-4 (subtropical scrublands). Overall, evergreen and deciduous forests (ECO-2) have the highest TINDVI at all latitudes, linked to their high elevation (Table 2), except near 24°N where they are similar to ECO-1. The consistently high TINDVI with latitude for ECO-2 is primarily due to high DUR. On the other extreme, ECO-5 (Sonoran Desert) has consistently low TINDVI, due to a high DUR and low ΔNDVI, with values that are only similar to ECO-4 from 30° to 32°N. This suggests that seasonal vegetation productivity in the NAM region is bounded by 1) high TINDVI values in evergreen and deciduous trees of the southern ECO-2 and 2) low TINDVI values in desert shrublands of northern ECO-5. Intermediate ecosystems (ECO-1 and ECO-4) exist within these bounds, greatly varying their TINDVI with latitudinal position, likely related to site-specific precipitation availability (Fig. 6) and the variations in an ecoregion of the plant phenology. Interestingly, the latitudinal variations of ECO-1 and ECO-4 in TINDVI are primarily due to changes in DUR as ΔNDVI decreases weakly with higher latitudes.

We also explore the effects of elevation, aspect, and slope on TINDVI, DUR, and ΔNDVI. For most ecoregions, aspect has a minimal impact on TINDVI, with the exception of ECO-2, which has a minor decrease on south-facing slopes (180° aspect) owing to a lower DUR. This suggests that this region does not have a strong aspect control on vegetation patterns at 8-km resolution. Note the positive relationship between TINDVI and slope in

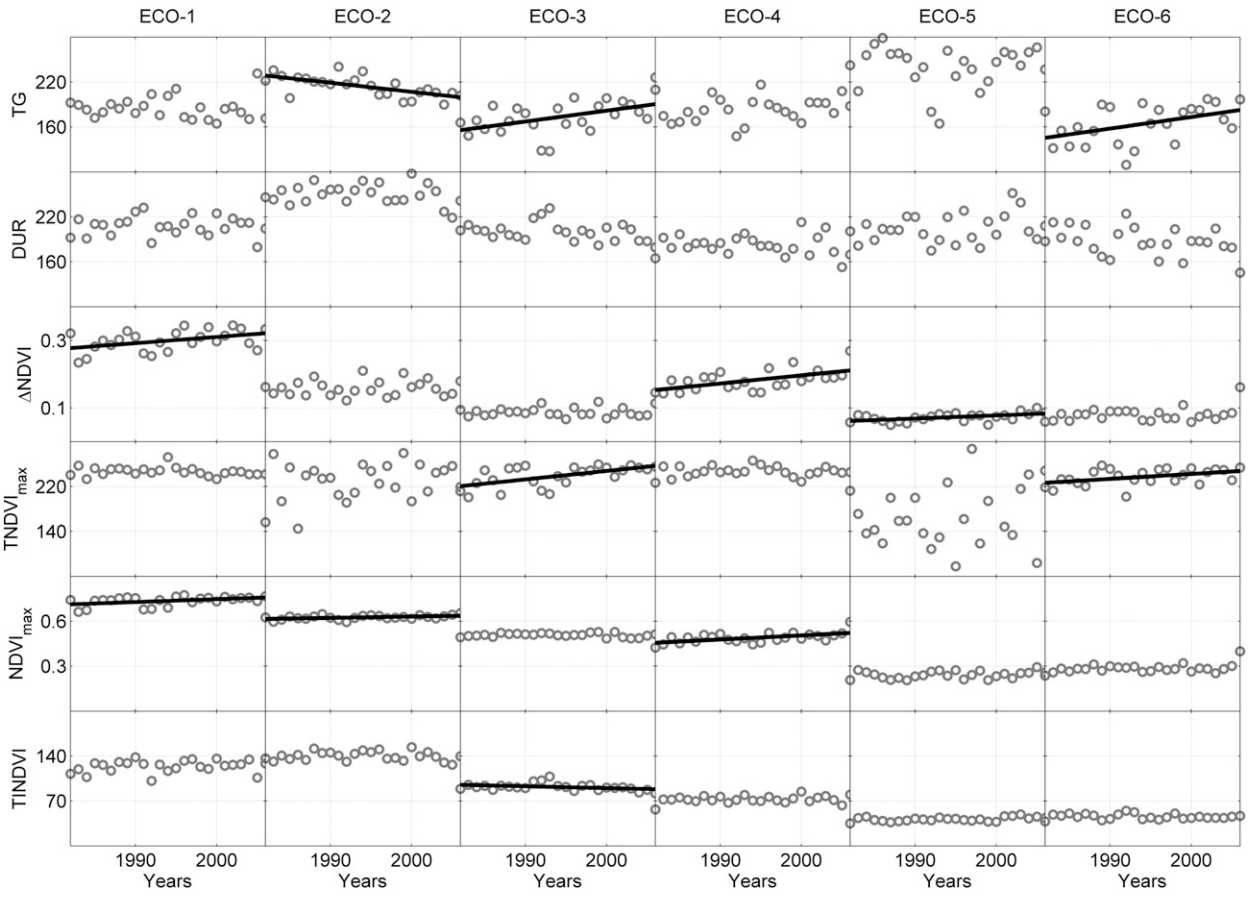

FIG. 10. Interannual variability of vegetation metrics for each ecoregion with statistically significant linear trends presented as thick lines.

each ecoregion, indicating that higher slope areas tend to have greater productivity (note that maximum slopes of 7° at 8 km are reduced with respect to actual slopes). For ECO-2, mountain forests have prolonged but moderate greening that grows steadily with higher slope due to higher ΔNDVI. While the dependence of TINDVI on slope is similar for ECO-1 (tropical dry forests), the underlying cause is very different: an increase in DUR with slope more than offsets the observed decrease in ΔNDVI. Over TOT, the predominant cause for higher TINDVI with slope appears to be ΔNDVI over the range of 0°–3° and DUR over the range of 3°–7°. These results suggest a complex interaction between slope and TINDVI involving adjustments within an ecoregion as well as ecoregion organization in the domain.

Elevation dependence of TINDVI varies according to the ecoregion: 1) ECO-1: moderate increase with elevation; 2) ECO-2: moderate decrease with elevation; 3) ECO-4: weak increase with elevation (note the high TINDVI for low altitude is due to agriculture); and 4) ECO-5: strong increase with elevation up to 1200 m with low values thereafter. It is important to keep in mind that stratifying by ecoregion limits the elevation dependence to within-class variability. TINDVI for TOT clearly increases with elevation primarily due to a higher DUR with altitude, even when ΔNDVI decreases with elevation. This is an interesting feature in each ecoregion and the overall spatial pattern that indicates preference for moderate and sustained greening at high elevations, while lower elevation sites are dominated by rapid greening of limited duration. Clearly, there should be an underlying set of abiotic factors, most likely precipitation characteristics (Gochis et al. 2007; Nesbitt et al. 2008), that drive these plant adaptations along mountain fronts. A detailed analysis of long-term precipitation data arranged along different elevation and vegetation zones could potentially aid in identifying these abiotic controls.

f. Long-term trends in vegetation phenological metrics

The long-term NDVI is used to explore linear trends in vegetation metrics as a first step to identifying climatic controls on the vegetation dynamics. Figure 10 shows the interannual variability for each ecoregion of TG, DUR,

TABLE 3. Statistical parameters of linear trends in annual vegetation metrics (Fig. 10), including p values and slopes. Note that $p < 0.05$ (boldface) highlights correlations that are significantly different from zero, thus the hypothesis of a linear trend cannot be rejected.

	TG		DUR		ΔNDVI		$TNDVI_{max}$		$NDVI_{max}$		TINDVI	
Ecoregion	p	slope	p	slope	p	slope	p	slope	p	slope	p	slope
ECO-1	0.218	−0.097	0.835	0.003	**0.036**	**0.001**	0.112	−0.227	**0.013**	**0.001**	0.275	0.282
ECO-2	**0**	**−1.209**	0.594	−0.287	0.728	0	0.282	1.347	**0.041**	**0**	0.871	−0.051
ECO-3	**0.022**	**1.448**	0.088	−0.575	0.763	0	**0.002**	**1.505**	0.944	0	**0.028**	**−0.28**
ECO-4	0.366	0.444	0.417	−0.206	**0.002**	**0.002**	0.799	0.105	**0.006**	**0.002**	0.627	0.185
ECO-5	0.944	0.06	0.366	0.689	**0.008**	**0**	0.513	1.66	0.201	0	0.051	0.214
ECO-6	**0.025**	**1.549**	0.051	−0.948	0.366	0	**0.036**	**0.875**	0.185	0.001	0.728	−0.071

ΔNDVI, $TNDVI_{max}$, $NDVI_{max}$, and TINDVI. Linear regressions (solid lines) are displayed only for those significant linear trends where p values are less than 0.05. Table 3 lists the slope of the linear regression and p values, with the significant trends in bold. Clearly, the interannual variations vary for different metrics and across the ecoregions. Significant linear trends are present in specific ecoregions for all metrics except DUR. However, it is important to note these trends are derived for ecoregion averages that aggregate the spatial variability within many pixels, with some having insignificant trends. To exhibit these spatial differences, Fig. 11 presents the slopes of the significant linear trends for each vegetation metric at the pixel scale. Along with ecoregion averages, spatial distributions allow interpretations of the long-term trends (if any) of the vegetation dynamics.

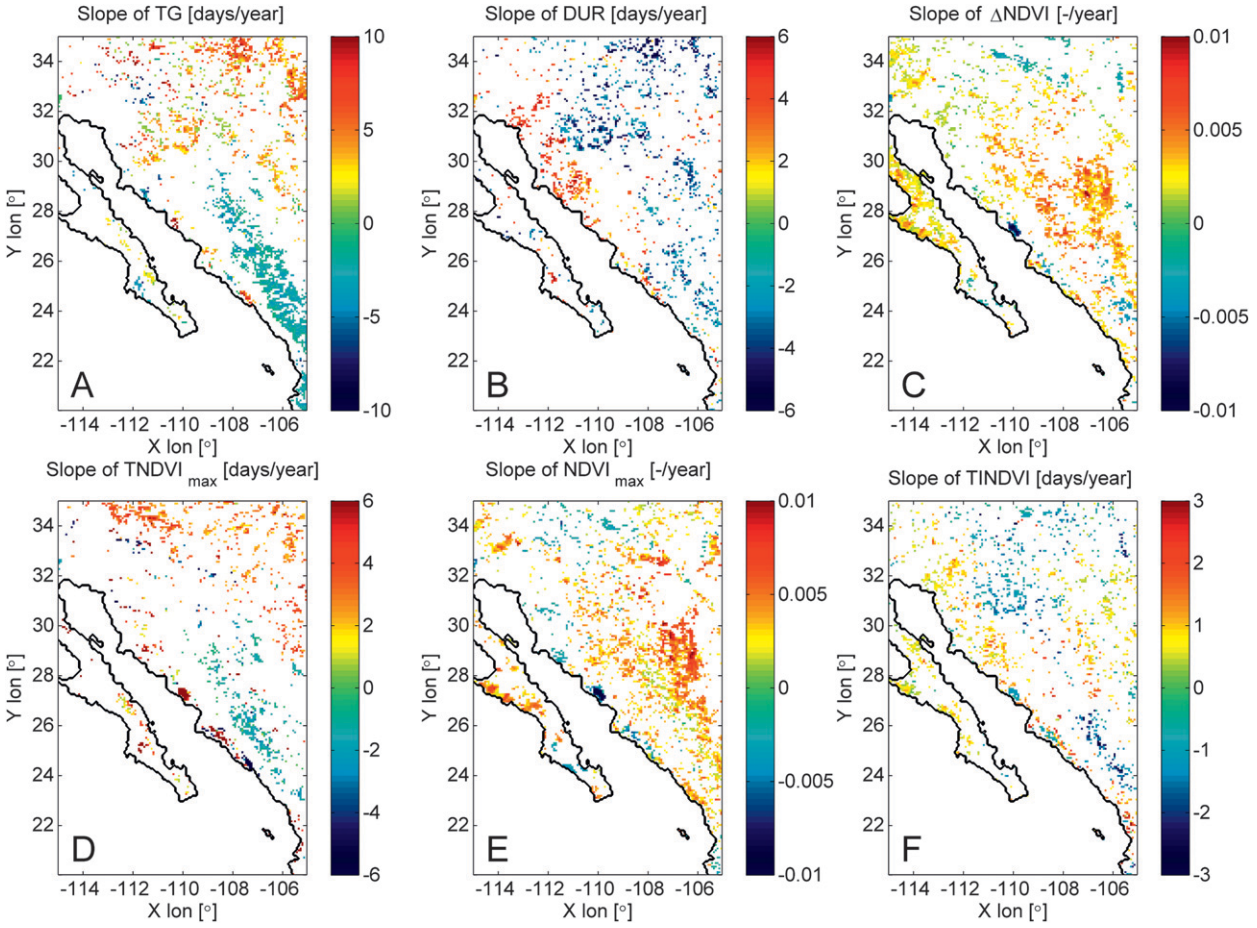

FIG. 11. Spatial maps of the linear trends of interannual changes of vegetation metrics for individual pixels: (a) TG, (b) DUR, (c) ΔNDVI, (d) $TNDVI_{max}$, (e) $NDVI_{max}$, and (f) TINDVI. White pixels represent areas where the Mann–Kendall test for a linear trend is not satisfied ($\rho = 0.05$).

The timing of TG varies among the ecoregions, with significant increasing trends in northern areas (ECO-3, ECO-6) and significant decreasing trends in southern areas (ECO-2). Figure 11a corroborates these ecoregion-averaged results and indicates a spatial difference in the sign of the linear trend between northern and southern areas with a separation near 30°N. This suggests that the northern conifer forest (ECO-3), Chihuahuan Desert areas (ECO-6), and portions of subtropical scrublands (ECO-4) are experiencing a delayed beginning (higher TG) of ~1.5–1.7 days yr^{-1} (Table 3), while southern evergreen and deciduous forests (ECO-2) exhibit an earlier greening (lower TG) of ~1.2 days yr^{-1}. Long-term trends in TG are not apparent in tropical dry forests (ECO-1) or the Sonoran Desert (ECO-5). Long-term trends in the greening onset should be related to differences in the arrival of NAM precipitation events over this period. For example, Grantz et al. (2007) showed a statistically significant delay in the NAM onset for Arizona and New Mexico during the period 1948–2004, consistent with the higher TG for ECO-3, ECO-6, and ECO-4. To our knowledge, a similar analysis has not been performed for the SMO (ECO-2 with lower TG) owing to the sparse long-term precipitation data at the appropriate resolution.

Interestingly, differences in TG are accompanied by simultaneous decreases in the greening duration (Fig. 11b) in pixels within ECO-2, ECO-3, ECO-4, and ECO-6, though no significant trends are observed in the ecoregion averages. The overall decreases in DUR are ~0.5–1 day yr^{-1}. This is consistent with decreasing trends in NAM duration for locations in Sonora and Arizona (Englehart and Douglas 2006). Longer greening durations are only found in Sonoran Desert areas (ECO-5), suggesting this region is experiencing a later greening TS since TG does not exhibit significant trends. Furthermore, a distinct spatial separation is observed between the mountainous ECO-4 and ECO-6 with shorter DUR and the coastal ECO-5 with a longer DUR. Note the long-term trends in TG and DUR are of greater magnitude and are more widespread spatially than any trends in the timing of the peak greenness ($TNDVI_{max}$, Fig. 11d). Overall, areas with later (earlier) TG also exhibit a delayed (advanced) $TNDVI_{max}$, an indication of a translation of the seasonal phenology in response to precipitation shifts during the NAM (e.g., Englehart and Douglas 2006; Grantz et al. 2007).

In contrast to vegetation timing, linear trends in $NDVI_{max}$ and $\Delta NDVI$, representing greening magnitude, are positive and consistent for most of the NAM region (Figs. 11c and 11e). Ecoregion metrics indicate a significant increasing linear trend in the maximum greenness for ECO-1, ECO-2, ECO-4, and ECO-6. For example, a large spatial region in ECO-4 exhibits increases in $NDVI_{max}$ of approximately 0.05 over the study period. These coherent trends, while limited in total magnitude, may be an indication of subtle changes in the spatial location of NAM precipitation. Furthermore, similarities in the spatial distribution of trends in $NDVI_{max}$ and $\Delta NDVI$ indicate that minimum NDVI values are relatively unaltered. It is interesting to note that, despite the significant linear trends in $NDVI_{max}$, there are weaker trends for TINDVI (Fig. 11f) and that the ecoregion averages exhibit variations in directionality. For example, pixels with conifers (ECO-3) and evergreen and deciduous forests (ECO-2) show decreases in TINDVI, while certain desert (ECO-5) and scrubland (ECO-4) areas have increasing TINDVI in time. This may be an indication of a long-term trend toward favorability of ecosystems that intensively utilize NAM precipitation for rapid productivity (i.e., deciduous plant strategies with high $NDVI_{max}$ and short DUR), as opposed to delayed production (i.e., evergreen plant strategies with low $NDVI_{max}$ and long DUR). A persistence of these trends could potentially result in the reorganization of ecoregions with geographic position and topographic attributes.

4. Summary and conclusions

In this study, we analyzed long-term (1982–2006) AVHRR NDVI observations to quantify the spatial and temporal vegetation dynamics in the North American monsoon region. This quantification is important from a climate perspective because of the hypothesized role played by land surface conditions on the dynamics of the NAM system via a vegetation–rainfall feedback mechanism (e.g., Matsui et al. 2005; Watts et al. 2007; Higgins and Gochis 2007; Dominguez et al. 2008; Castro et al. 2009; Méndez-Barroso and Vivoni 2010). From a hydrologic perspective, quantifying vegetation dynamics in the NAM region is critical for (i) inferring the spatial distribution of precipitation and soil moisture in sparsely gauged regions (e.g., Gochis et al. 2007; Nesbitt et al. 2008; Méndez-Barroso et al. 2009) and (ii) incorporating vegetation phenology into improved seasonal forecasts of soil moisture, evapotranspiration, and streamflow (e.g., Vivoni et al. 2008a; Vivoni et al. 2010b).

An important motivation for quantifying vegetation dynamics is the recent evidence obtained during NAME on the variation of precipitation characteristics with elevation and its implications on ecosystem patterns. As shown by Gochis et al. (2007), Gebremichael et al. (2007), and Nesbitt et al. (2008), high-elevation sites with evergreen woodlands typically experience more frequent, but less intense, precipitation events as compared to lower-elevation sites in deciduous ecosystems. As a result, it is possible that vegetation patterns in the NAM region are a result of variations in the soil water balance

arising from elevation gradients in precipitation characteristics and in temperature regimes. This study lays a foundation to test this climate–ecosystem organization hypothesis by quantifying the spatiotemporal dynamics of vegetation at the remotely sensed pixel and ecoregion scales.

This study has characterized several important features of the spatiotemporal variability of vegetation dynamics in the NAM region, including the identification of the following: 1) distinct ecoregions with coherent vegetation variability; 2) spatial patterns in vegetation phenological metrics and their ecoregion dependence; 3) variations with geographic location and topographic attributes; and 4) interannual variability at the ecoregion and pixel scales, including an assessment of significant long-term linear trends. Based on these complementary analyses, the major findings of this study can be synthesized by comparing the seasonal biomass productivity, as captured by vegetation metrics, in two distinct ecosystem types. These cases represent different plant strategies (deciduous versus evergreen) whose occurrence varies along spatial gradients to cope with seasonal and interannual water availability:

1) Deciduous ecosystems (e.g., semiarid grasslands, subtropical scrublands, tropical dry forests) have a high seasonality during a short period of intense greening occurring rapidly after the NAM precipitation onset.
2) Evergreen ecosystems (e.g., mountain woodlands, conifer forests) have a more muted seasonality during a prolonged period of moderate greenness that is delayed with respect to precipitation onset but continues after the NAM.

Interannual precipitation variability leads to divergent vegetation responses from the two ecosystem types, with a greater adjustment in the greening range for deciduous plants and a larger modification of the greening duration and peak timing for evergreen forests. With changes in water availability in space (e.g., latitude, elevation), the two ecosystem types have similar directional responses but of different magnitudes. At low latitudes, the greening duration is increased highly (modestly) in deciduous (evergreen) ecosystems, while greening range is increased modestly (highly). For higher elevations, increases in greening duration are sufficiently large in both ecosystems to overcome decreases in the range of greening. Clearly, ecosystem differences should be considered when analyzing seasonal biomass productivity, as different plant strategies exist for greening range (deciduous) and duration (evergreen). Long-term trends in vegetation metrics also indicate higher greening ranges for deciduous ecosystems and lower greening durations for evergreen ecosystems. A persistence of these trends could potentially result in the spatial reorganization of ecosystems in the NAM region.

Acknowledgments. We thank H2CU for the financial support of G.F. during a visiting period with E.R.V. We also acknowledge funding for E.R.V. from the NOAA Climate Program Office (Grant CPPA GC07-019) and the U.S. Fulbright Scholar program. We thank Luis A. Méndez-Barroso and Giuseppe Mascaro for discussions related to this work.

REFERENCES

Alcaraz-Segura, D., E. Liras, S. Tabik, J. Paruelo, and J. Cabello, 2010: Evaluating the consistency of the 1982–1999 NDVI trends in the Iberian Peninsula across four time series derived from the AVHRR sensor: LTDR, GIMMS, FASIR, and PAL-II. *Sensors,* **10,** 1291–1314.

Alessandri, A., and A. Navarra, 2008: On the coupling between vegetation and rainfall inter-annual anomalies: Possible contributions to seasonal rainfall predictability over land areas. *Geophys. Res. Lett.,* **35,** L02718, doi:10.1029/2007GL032415.

Anderson, B. T., H. Kanamura, and J. O. Roads, 2004: The summertime atmospheric hydrologic cycle over the southwestern United States. *J. Hydrometeor.,* **5,** 679–692.

Armstrong, R. N., and L. W. Martz, 2003: Topographic parameterization in continental hydrology: A study in scale. *Hydrol. Processes,* **17,** 3763–3781.

Brito-Castillo, L., E. R. Vivoni, D. J. Gochis, A. Filonov, I. Tereshchenko, and C. Monzon, 2010: An anomaly in the occurrence of the month of maximum precipitation distribution in northwest Mexico. *J. Arid Environ.,* **74,** 531–539.

Brown, D. E., 1994: *Biotic Communities: Southwestern United States and Northwestern Mexico*. University of Utah Press, 342 pp.

Buermann, W., Y. Wang, J. Dong, L. Zhou, X. Zeng, R. E. Dickinson, C. S. Potter, and R. B. Myneni, 2002: Analysis of a multiyear global vegetation leaf area index data set. *J. Geophys. Res.,* **107,** 4646, doi:10.1029/2001JD000975.

Buyantuyev, A., and J. Wu, 2009: Urbanization alters spatiotemporal patterns of ecosystem primary production: A case study of Phoenix metropolitan region, USA. *J. Arid Environ.,* **73,** 512–520.

Caparrini, F., F. Castelli, and D. Entekhabi, 2003: Mapping of land–atmosphere heat fluxes and surface parameters with remote sensing data. *Bound.-Layer Meteor.,* **107,** 605–633.

Caso, M., C. Gonzalez-Abraham, and E. Ezcurra, 2007: Divergent ecological effects of oceanographic anomalies on terrestrial ecosystems of the Mexican Pacific coast. *Proc. Natl. Acad. Sci. USA,* **104,** 10 530–10 535.

Castro, C. L., A. B. Beltran-Przekurat, and R. A. Pielke, 2009: Spatiotemporal variability of precipitation, modeled soil moisture, and vegetation greenness in North America within the recent observational record. *J. Hydrometeor.,* **10,** 1355–1378.

Chen, X. F., J. M. Chen, S. Q. An, and W. M. Ju, 2007: Effects of topography on simulated net primary productivity at landscape scale. *J. Environ. Manage.,* **85,** 585–596.

Coblentz, D. D., and K. H. Riitters, 2004: Topographic controls on the regional-scale biodiversity of the south-western USA. *J. Biogeogr.,* **31,** 1125–1138.

Commission for Environmental Cooperation, 1997: *Ecological Regions of North America*. CEC, 71 pp.

Deng, Y. X., X. F. Chen, E. Chuvieco, T. Warner, and J. P. Wilson, 2007: Multiscale linkages between topographic attributes and vegetation indices in a mountainous landscape. *Remote Sens. Environ.,* **111,** 122–134.

Dominguez, F., P. Kumar, and E. R. Vivoni, 2008: Precipitation recycling variability and ecoclimatological stability—A study using NARR data. Part II: North American monsoon region. *J. Climate,* **21,** 5187–5203.

Douglas, M. W., R. A. Maddox, K. Howard, and S. Reyes, 1993: The Mexican monsoon. *J. Climate,* **6,** 1665–1677.

Eagleson, P. S., 2002: *Ecohydrology: Darwinian Expression of Vegetation Form and Function*. Cambridge University Press, 443 pp.

Englehart, P. J., and A. V. Douglas, 2006: Defining intraseasonal rainfall variability within the North American monsoon. *J. Climate,* **19,** 4243–4253.

Forzieri, G., F. Castelli, and E. R. Vivoni, 2010: A predictive multidimensional model of vegetation anomalies derived from remote-sensing observations. *IEEE Trans. Geosci. Remote Sens.,* **48,** 1729–1741.

Gebremichael, M., E. R. Vivoni, C. J. Watts, and J. C. Rodríguez, 2007: Submesoscale spatiotemporal variability of North American monsoon rainfall over complex terrain. *J. Climate,* **20,** 1751–1773.

Gochis, D. J., A. Jimenez, C. J. Watts, J. Garatuza-Payán, and W. J. Shuttleworth, 2004: Analysis of 2002 and 2003 warm season precipitation from the North American Monsoon Experiment event rain gauge network. *Mon. Wea. Rev.,* **132,** 2938–2953.

——, C. J. Watts, J. Garatuza-Payán, and J. C. Rodríguez, 2007: Spatial and temporal patterns of precipitation intensity as observed by the NAME event rain gauge network from 2002 to 2004. *J. Climate,* **20,** 1734–1750.

Gómez-Mendoza, L., L. Galicia, M. L. Cuevas-Fernandez, V. Magana, G. Gómez, and J. L. Palacios-Prieto, 2008: Assessing onset and length of greening period in six vegetation types in Oaxaca, Mexico, using NDVI-precipitation relations. *Int. J. Biometeor.,* **52,** 511–520.

Grantz, K., B. Rajagopalan, M. Clark, and E. Zagona, 2007: Seasonal shifts in the North American monsoon. *J. Climate,* **20,** 1923–1935.

Gutman, G., and A. Ignatov, 1998: The derivation of the green vegetation fraction from NOAA/AVHRR data for use in numerical weather prediction models. *Int. J. Remote Sens.,* **19,** 1533–1542.

Gutzler, D. S., 2004: An index of interannual precipitation variability in the core of the North American monsoon region. *J. Climate,* **17,** 4473–4480.

Higgins, R. W., and W. Shi, 2001: Intercomparison of the principal modes of interannual and intraseasonal variability of the North American monsoon system. *J. Climate,* **14,** 403–417.

——, and D. J. Gochis, 2007: Synthesis of results from the North American Monsoon Experiment (NAME) process study. *J. Climate,* **20,** 1601–1607.

Hirosawa, Y., S. E. Marsh, and D. H. Kliman, 1996: Application of standardized principal component analysis to land-cover characterization using multitemporal AVHRR data. *Remote Sens. Environ.,* **58,** 267–281.

Hong, Y., D. Gochis, J. T. Cheng, K. L. Hsu, and S. Sorooshian, 2007: Evaluation of the PERSIANN-CCS rainfall measurement using the NAME event rain gauge network. *J. Hydrometeor.,* **8,** 469–482.

Ivanov, V. Y., R. L. Bras, and E. R. Vivoni, 2008: Vegetation-hydrology dynamics in complex terrain of semiarid areas. I. A mechanistic approach to modeling dynamic feedbacks. *Water Resour. Res.,* **44,** W03429, doi:10.1029/2006WR005588.

Jenerette, G. D., R. L. Scott, and A. R. Huete, 2010: Functional differences between summer and winter season rain assessed with MODIS-derived phenology in a semi-arid region. *J. Veg. Sci.,* **21,** 16–30.

Kaufmann, R. K., L. Zhou, Y. Knyazikhin, N. V. Shabanov, R. B. Myneni, and C. J. Tucker, 2000: Effect of orbital drift and sensor changes on the time series of AVHRR vegetation index data. *IEEE Trans. Geosci. Remote Sens.,* **38,** 2584–2597.

Li, Z., and M. Kafatos, 2000: Interannual variability of vegetation in the United States and its relation to El Nino/Southern Oscillation. *Remote Sens. Environ.,* **71,** 239–247.

Lillesand, T. M., R. W. Kiefer, and J. W. Chipman, 2008: *Remote Sensing and Image Interpretation*. 6th ed. John Wiley & Sons, 784 pp.

Lizárraga-Celaya, C., C. J. Watts, J. C. Rodríguez, J. Garatuza-Payán, R. L. Scott, and J. A. Sáiz-Hernández, 2010: Spatiotemporal variations in surface characteristics over the North American Monsoon region. *J. Arid Environ.,* **74,** 540–548.

Lotsch, A., M. A. Friedl, B. T. Anderson, and C. J. Tucker, 2005: Response of terrestrial ecosystems to recent Northern Hemispheric drought. *Geophys. Res. Lett.,* **32,** L06705, doi:10.1029/2004GL022043.

MacQueen, J. B., 1967: Some methods for classification and analysis of multivariate observations. *Proceedings of Fifth Berkeley Symposium on Mathematical Statistics and Probability,* University of California Press, 281–297.

Maignan, F., F. M. Breon, C. Bacour, J. Demarty, and A. Poirson, 2008: Interannual vegetation phenology estimates from global AVHRR measurements—Comparison with in situ data and applications. *Remote Sens. Environ.,* **112,** 496–505.

Matsui, T., V. Lakshmi, and E. E. Small, 2005: The effects of satellite-derived vegetation cover variability on simulated land–atmosphere interactions in the NAMS. *J. Climate,* **18,** 21–40.

Méndez-Barroso, L. A., and E. R. Vivoni, 2010: Observed shifts in land surface conditions during the North American monsoon: Implications for a vegetation–rainfall feedback mechanism. *J. Arid Environ.,* **74,** 549–555.

——, J. Garatuza-Payán, and E. R. Vivoni, 2008: Quantifying water stress on wheat using remote sensing in the Yaqui Valley, Sonora, Mexico. *Agric. Water Manage.,* **95,** 725–736.

——, E. R. Vivoni, C. J. Watts, and J. C. Rodríguez, 2009: Seasonal and interannual relations between precipitation, surface soil moisture and vegetation dynamics in the North American monsoon region. *J. Hydrol.,* **377,** 59–70.

Mesinger, F., and Coauthors, 2006: North American regional reanalysis. *Bull. Amer. Meteor. Soc.,* **87,** 343–360.

Mora, F., and L. R. Iverson, 1998: On the sources of vegetation activity variation, and their relation with the water balance in Mexico. *Int. J. Remote Sens.,* **19,** 1843–1871.

Myneni, R. B., S. O. Los, and C. J. Tucker, 1996: Satellite-based identification of linked vegetation index and sea surface temperature anomaly areas from 1981–1990 for Africa, Australia and South America. *Geophys. Res. Lett.,* **23,** 729–732.

Nesbitt, S. W., D. J. Gochis, and T. J. Lang, 2008: The diurnal cycle of clouds and precipitation along the Sierra Madre Occidental observed during NAME-2004: Implications for warm season precipitation estimation in complex terrain. *J. Hydrometeor.,* **9,** 728–743.

Notaro, M., Z. Liu, and J. W. Williams, 2006: Observed vegetation–climate feedback in the United States. *J. Climate,* **19,** 763–786.

Pennington, D. D., and S. L. Collins, 2007: Response of an aridland ecosystem to interannual climate variability and prolonged drought. *Landscape Ecol.,* **22,** 897–910.

Pérez-Ruiz, E., J. Garatuza-Payán, C. J. Watts, J. C. Rodríguez, E. A. Yépez, and R. L. Scott, 2010: Carbon dioxide and water vapor exchange in a tropical dry forest as influenced by the North American Monsoon System (NAMS). *J. Arid Environ.,* **74,** 556–563.

Pielke, R. A., R. Avissar, M. Raupach, A. J. Dolman, X. Zeng, and A. S. Denning, 1998: Interactions between the atmosphere and terrestrial ecosystems: Influence on weather and climate. *Glob. Change Biol.,* **4,** 461–475.

Pinzon, J., M. E. Brown, and C. J. Tucker, 2005: Satellite time series correction of orbital drift artifacts using empirical mode decomposition. *Hilbert-Huang Transform: Introduction and Applications,* N. Huang, Ed., World Scientific, 167–186.

Reed, B. C., J. F. Brown, D. VanderZee, T. R. Loveland, J. W. Merchant, and D. O. Ohlen, 1994: Measuring phenological variability from satellite imagery. *J. Veg. Sci.,* **5,** 703–714.

Riera, J. L., J. T. Magnuson, J. R. V. Castle, and M. D. MacKenzie, 1998: Analysis of large-scale spatial heterogeneity in vegetation indices among North American landscapes. *Ecosystems (N. Y.),* **1,** 268–282.

Salinas-Zavala, C. A., A. V. Douglas, and H. F. Díaz, 2002: Interannual variability of NDVI in northwest Mexico: Associated climatic mechanisms and ecological implications. *Remote Sens. Environ.,* **82,** 417–430.

Tucker, C. J., J. E. Pinzon, and M. E. Brown, 2004: Global inventory modeling and mapping studies. Global Land Cover Facility, University of Maryland, College Park, Rep. NA94apr15b. n11-VIg, 2.0.

——, ——, ——, D. Slayback, E. W. Pak, R. Mahoney, E. Vermote, and N. Saleous, 2005: An extended AVHRR 8-km NDVI data set compatible with MODIS and SPOT vegetation NDVI data. *Int. J. Remote Sens.,* **26,** 4485–4498.

Verdin, K., and J. Verdin, 1999: A topological system for the delineation and codification of the Earth's river basins. *J. Hydrol.,* **218,** 1–12.

Vivoni, E. R., V. Y. Ivanov, R. L. Bras, and D. Entekhabi, 2004: Generation of triangulated irregular networks based on hydrological similarity. *J. Hydrol. Eng.,* **9,** 288–302.

——, and Coauthors, 2007: Variation of hydrometeorological conditions along a topographic transect in northwestern Mexico during the North American monsoon. *J. Climate,* **20,** 1792–1809.

——, H. A. Moreno, G. Mascaro, J. C. Rodríguez, C. J. Watts, J. Garatuza-Payán, and R. L. Scott, 2008a: Observed relation between evapotranspiration and soil moisture in the North American monsoon region. *Geophys. Res. Lett.,* **35,** L22403, doi:10.1029/2008GL036001.

——, M. Gebremichael, C. J. Watts, R. Bindlish, and T. J. Jackson, 2008b: Comparison of ground-based and remotely sensed surface soil moisture estimates over complex terrain during SMEX04. *Remote Sens. Environ.,* **112,** 314–325.

——, C. J. Watts, and D. J. Gochis, 2010a: Land surface ecohydrology of the North American monsoon system. *J. Arid Environ.,* **74,** 529–530.

——, J. C. Rodriguez, and C. J. Watts, 2010b: On the spatiotemporal variability of soil moisture and evapotranspiration in a mountainous basin within the North American monsoon region. *Water Resour. Res.,* **46,** W02509, doi:10.1029/2009WR008240.

——, C. J. Watts, J. C. Rodríguez, J. Garatuza-Payán, L. A. Méndez-Barroso, and J. A. Sáiz-Hernández, 2010c: Improved land–atmosphere relations through distributed footprint measurements in a subtropical scrubland during the North American monsoon. *J. Arid Environ.,* **74,** 579–584.

Watts, C. J., R. L. Scott, J. Garatuza-Payán, J. C. Rodríguez, J. H. Prueger, W. P. Kustas, and M. Douglas, 2007: Changes in vegetation condition and surface fluxes during NAME 2004. *J. Climate,* **20,** 1810–1820.

Weiss, J. L., D. S. Gutzler, J. E. A. Coonrod, and C. N. Dahm, 2004: Long-term vegetation monitoring with NDVI in a diverse semi-arid setting, central New Mexico, USA. *J. Arid Environ.,* **58,** 249–272.

White, A. B., P. Kumar, and D. Tcheng, 2005: A data mining approach for understanding topographic control on climate interannual vegetation variability over the United States. *Remote Sens. Environ.,* **98,** 1–20.

White, M. A., P. E. Thorton, and S. W. Running, 1997: A continental phenology model for monitoring vegetation responses to interannual climatic variability. *Global Biogeochem. Cycles,* **11,** 217–234.

Wilks, D. S., 1995: *Statistical Methods in the Atmospheric Sciences—An Introduction.* International Geophysics Series, Vol. 59, Academic Press, 467 pp.

Zeng, X. B., P. Rao, R. S. DeFries, and M. C. Hansen, 2003: Interannual variability and decadal trend of global fractional vegetation cover from 1982 to 2000. *J. Appl. Meteor.,* **42,** 1525–1530.

Zhang, X. Y., M. A. Friedl, C. B. Schaaf, A. H. Strahler, J. C. F. Hodges, F. Gao, B. C. Reed, and A. Huete, 2003: Monitoring vegetation phenology using MODIS. *Remote Sens. Environ.,* **84,** 471–475.

Zhu, C., and D. P. Lettenmaier, 2007: Long-term climate and derived surface hydrology and energy flux data for Mexico: 1925–2004. *J. Climate,* **20,** 1936–1946.